



# North Atlantic Oscillation (NAO) in the Paleoclimate Modelling Intercomparison Project (PMIP)

Anni Zhao<sup>1</sup>, Chris Brierley<sup>2</sup>, Venni Arra-Kastrati<sup>2</sup>, Xiaoxu Shi<sup>3</sup>, and Yongyun Hu<sup>1</sup>

<sup>1</sup>Department of Atmospheric and Oceanic Sciences, School of Physics, Peking University, Beijing, 100871, China

<sup>2</sup>Department of Geography, University College London, London, WC1E 6BT, UK

<sup>3</sup>Southern Marine Science and Engineering Guangdong Laboratory (Zhuhai), Zhuhai, 519082, China

**Correspondence:** Yongyun Hu (yyhu@pku.edu.cn)

Received: 1 July 2025 – Discussion started: 22 July 2025

Revised: 2 March 2026 – Accepted: 11 March 2026 – Published: 30 March 2026

**Abstract.** The North Atlantic Oscillation (NAO) is one of the main modes of climate variability and the dominant mode of large-scale atmospheric variability in the North Atlantic basin and has large impacts on the European climate, yet the behaviour of NAO in the future remains uncertain. Here we assess the NAO response in the past and in a warming climate by looking at a comprehensive set of coupled model simulations performed by the Paleoclimate Model Intercomparison Project (PMIP) and the Coupled Model Intercomparison Project (CMIP) for four experiments: the mid-Holocene (6 ka; *midHolocene*), the Last Glacial Maximum (21 ka; *lgm*), the Last Interglacial (127 ka; *lig127k*) and an idealised greenhouse gas (GHG)-forced experiment from the CMIP DECK with abrupt quadrupled CO<sub>2</sub> (*abrupt4xCO2*). Although there are various setups across experiments, the *midHolocene* and *lig127k* are mainly characterised by altered orbital configurations, inducing variations in the seasonal cycle and redistributing energy across latitudes. The *lgm* and *abrupt4xCO2* are characterised by GHG forcings that induce substantial global temperature change, and the *lgm* includes large ice sheets that alter the storm-tracks. Our results show that the NAO alters in these latter two experiments, but is not sensitive to the orbital configurations. NAO weakens in response to cooling and strengthens as a result of warming. The associated teleconnections change consistently with the theory and are sensitive to the change in NAO amplitude. The two orbital experiments do not show a clear change in associated temperature and precipitation. The weakened NAO in the *lgm* is associated with a cooler and drier northern Europe, while the enhanced NAO in the *abrupt4xCO2* causes a warmer and wetter northern Europe as compared to the *pi-*

*Control*. No clear relationship is found in the ENSO-NAO teleconnection.

## 1 Introduction

The North Atlantic Oscillation (NAO) represents one of the main modes of climate variability and the dominant mode of large-scale atmospheric variability in the North Atlantic basin (Hurrell et al., 2003), which affects regional climate (Woollings et al., 2015) – most pronounced during boreal winter (Walker and Bliss, 1932). NAO is defined by two commonly used frameworks: the principal component (PC) as the leading empirical orthogonal function (EOF) of sea level pressure (SLP) variance during boreal winter over the North Atlantic-Europe sector (IPCC, 2021b), or based on observations from fixed locations such as the difference of normalised SLP anomalies between stations located in the Azores-Ponta Delgada and Iceland (Jones et al., 1997) or the difference between London and Paris (Cornes et al., 2013). This study adopts the PC-based definition to ensure consistency with large-scale circulation analyses. Characterised by seesaw sea level pressure anomalies between the Icelandic Low and the Azores High, the relative strength and spatial configuration of the two pressure centres determine the phase and intensity of the NAO. The positive phase of the NAO is formed by a deepening of the subpolar low (Iceland low) and strengthening of the subtropical high (Azores high), while its negative phase shows the opposite.

The interplay between the two pressure systems creates a pressure gradient that influences the temperature and precip-

itation variability over the North Atlantic and Eurasia, and the strength and direction of westerly winds and storm tracks across the North Atlantic (Woollings et al., 2014). The positive phase of the NAO, with enhanced pressure gradient, leads to an enhanced and northward shift of the jet stream, strengthened trade winds, and a northward shift of extratropical storms, which typically results in a warmer and wetter northern Europe and a colder and drier Mediterranean. Conversely, the negative phase of the NAO shows the reverse change in pressure systems, leading to a wavier jet stream that extends southward and a southward shift of storms, resulting in a colder northern Europe and a warmer southern Europe.

NAO variability is driven by multi-scale mechanisms, which can be categorized into internal dynamics and external forcings. Internally, NAO is predominantly driven by the internal atmospheric variability of mid-latitude dynamics (Lorenz and Hartmann, 2003) related to the interaction between eddy-mean flow (Feldstein and Franzke, 2017; Kimoto et al., 2001) and the coupling between troposphere and stratosphere (Wang and Ting, 2022; Omrani et al., 2022), and the coupling among atmosphere, land, and ocean (Marshall et al., 2001). External forcings include sea surface temperature (SST) (Mosedale et al., 2006; Hurrell et al., 2004), greenhouse gas (GHG) forcing (Stephenson et al., 2006; Barnes and Polvani, 2013), sea ice (Pedersen et al., 2016; Smith et al., 2017), and snow cover changes (Henderson et al., 2018; Spencer and Essery, 2016). In paleoclimate contexts, additional forcings such as altered orbital configuration (e.g., during the mid-Holocene (MH; 6 ka) and the Last Interglacial (LIG; 127 ka) and ice sheet topography (e.g., during the Last Glacial Maximum (LGM; 21 ka)) also affect NAO behaviours (Lü et al., 2010; Otto-Bliesner et al., 2006). Specifically, Justino and Peltier (2005) demonstrated that topographic forcing and ice-albedo feedback associated with the Laurentide and Scandinavian Ice Sheets during the LGM are crucial for generating distinct atmospheric variability patterns.

Several studies have carried out proxy-based reconstructed NAO (e.g. Vinther et al., 2003; Cook et al., 2019), though the reconstructions are limited by significant uncertainties arising from the limitations of archives and chronologies (Hernández et al., 2020), diverse methodologies (Michel et al., 2020), or the time scale effect on NAO variability (Woollings et al., 2015). For example, a positive NAO-like configuration was suggested during the mid-Holocene (MH; 6 ka) based on reconstructed terrestrial temperature over Europe (Mauri et al., 2014) and SSTs (Rimbu et al., 2003).

Earlier studies have explored the NAO in model simulations; however, the exact behaviour of NAO remains uncertain. The MH simulations from the Palaeoclimate Modelling Intercomparison Project 2 (PMIP2) show diverse changes in NAO variability relative to pre-industrial (PI) conditions, with studies reporting reduced variability (Lü et al., 2010), no change (Otto-Bliesner et al., 2006), or enhanced variability

(Gladstone et al., 2005). The results of the PMIP3 are also model-dependent (Găinușă-Bogdan et al., 2020). Under the cooler-than-present condition of the LGM, simulations show that the NAO pattern and variability weaken drastically in simulations, and the centres of the NAO pattern shift southward compared to both the PI and the MH (Lü et al., 2010; Otto-Bliesner et al., 2006). Future simulations predict a more positive mean state of the NAO index, although the response is highly model dependent (Miller et al., 2006; Osborn, 2004; Bader et al., 2011). As compared to averages from 1995–2014, the mean state of the NAO index is projected to shift towards being more predominantly in its positive phase under high-emission scenarios and has less robust change under low-emission scenarios by the end of the 21st century, with a large diversity across the Coupled Model Intercomparison Project (CMIP) simulations (Lee et al., 2021). The large spread is partly due to the contrasting influences of the negative phase of the NAO induced by Arctic amplification (Harvey et al., 2015; Peings et al., 2017; Screen et al., 2018) and the positive phase associated with enhanced warming in the tropical upper-troposphere (Vallis et al., 2015) in particular models in response to anthropogenic forcing (Harvey et al., 2014, 2015; Vallis et al., 2015; Oudar et al., 2017). McKenna and Maycock (2021) suggested that model structural differences contribute to two-thirds of the spread and internal variability to the rest in future NAO projections.

Research around changes in the NAO involves some confusing terminology, e.g., distinguishing NAO indices from mean state shifts vs. variability changes. Here, we adopt the definition of NAO as the leading EOF of December–January–February (DJF) SLP anomalies and consider the NAO to be a mode of variability, which can be described by the inter-annual changes in the NAO index (see Sect. 2 for details). Changes in the mean state of the Icelandic Low and Azores High will also project onto the pattern of that mode of variability – leading to secular shifts in the NAO index (i.e., shift in the mean state of the NAO), even if the oscillation itself remains the same. These are easy to distinguish in equilibrated climate model experiments, such as those used here. However, it is harder when looking at continuous NAO indices that capture a large range of frequencies, such as from palaeoclimate reconstructions or long transient simulations. Issues around lining up chronologies mean that capturing synchronous year-to-year spatial variations in NAO from reconstruction compilations is a substantial challenge.

In this study, we assess NAO change through time and NAO's response to distinct forcings based on the analysis of the PMIP3 and PMIP4 simulations. Four experiments are analyzed: orbitally dominated *midHolocene* for the MH and *lig127k* for the LIG – characterized by altered seasonal insolation with minor GHG adjustments; GHG/ice-sheet dominated *lgm* for the LGM-characterised by low GHG concentrations and large ice sheets; and an idealized warm experiment with quadrupled CO<sub>2</sub> from CMIP DECK (*abrupt4xCO2*). Section 2 introduces the models, experimen-

tal design, and analysis methods. A comparison between the *piControl* experiment with observation is provided in Sect. 3 for model evaluation. Section 4 describes changes in the mean state relative to the *piControl*. Section 5 presents the description of the change in NAO and the associated discussion. NAO teleconnections change, and discussion is given in Sect. 6. A brief conclusion is provided at the end as Sect. 7. Comparison between PMIP simulations with proxy data is not the aim of this study, and it has been done in assessing single experiments (see Brierley et al., 2020; Otto-Bliesner et al., 2021; Kageyama et al., 2021), so it will not be discussed in detail below.

## 2 Methods

This study involves a group of simulations across 2 CMIP/PMIP generations, 5 experiments, and 34 climate models (Table 1). Studies on individual experiments (Brierley et al., 2020; Otto-Bliesner et al., 2021; Kageyama et al., 2021) and single-model evaluations have been done by model groups (e.g. Otto-Bliesner et al., 2020). Therefore, we will keep the description of models and experimental design brief here, whilst references will be provided to find details.

### 2.1 Models

The CMIP has become a significant international multi-model research activity to investigate the Earth system response to forcing, evaluating the state-of-the-art coupled global climate models and assessing future climate changes and their uncertainties in scenarios (Eyring et al., 2016; Taylor et al., 2012). Simulations from the PMIP look at the past and serve as out-of-sample tests to study the roles of forcings and their feedbacks that establish the palaeoclimate and to evaluate the performance of models that are used to project future climate changes (Kageyama et al., 2018). Here, we choose the models that have completed the *piControl* simulations and at least one of the PMIP simulations (see Sect. 2.2) and have provided monthly surface temperature, precipitation and SLP for at least 30 years for all the simulations. Table 1 lists the 34 chosen models and their participation in the six experiments (see Sect. 2.2). Further details of the model design can be found in the listed references in Table 1 here, Table 9A.1 of Flato et al. (2013) for the CMIP5 models and Table AII.5 of IPCC (2021a) for the CMIP6 models.

### 2.2 Experimental design

This study uses simulations from five experiments with the protocols defined under the CMIP (Taylor et al., 2012; Eyring et al., 2016) or the PMIP (Kageyama et al., 2018): a PI control, one idealised CO<sub>2</sub>-forced future warming experiment and three past climate experiments, which include a colder *lgm* and two altered orbital configurations *midHolocene* and

*lig127k*. Model participation in each experiment is detailed in Table 1.

The DECK *piControl* was performed by all selected models, employing coupled atmosphere-ocean and boundary conditions approximately constant to 1850CE (Eyring et al., 2016). Depending on the individual model design, aerosol, vegetation, and ice sheet configurations are either interactive or prescribed as modern conditions. The CMIP6 *piControl* uses more realistic GHG concentrations (284.3 ppm, 808.2 ppb and 273 ppb for the atmospheric CO<sub>2</sub>, NH<sub>4</sub> and N<sub>2</sub>O concentrations, respectively) and a lower solar constant (1360.747 W m<sup>-2</sup>) compared to its earlier generation, the CMIP5, which set the atmospheric CO<sub>2</sub>, NH<sub>4</sub> and N<sub>2</sub>O concentrations at 280 ppm, 760 ppb and 270 ppb, respectively, and the solar constant at 1365 W m<sup>-2</sup>. The *piControl* serves as a baseline for assessing changes in other experiments. Model groups run their *piControl* simulations for a few hundred to a few thousand model years to reach an equilibrium state.

The idealised CO<sub>2</sub>-forced experiment, *abrupt4xCO2*, is also a requirement of the DECK CMIP experiments (Eyring et al., 2016). It is designed to reveal the basic feedback response of a model to high GHG forcing (Eyring et al., 2016) by having the atmospheric CO<sub>2</sub> concentration suddenly and immediately quadruple relative to the 1850 CE condition prescribed in the *piControl* at the beginning, and then maintaining constant (Eyring et al., 2016). The *abrupt4xCO2* simulations enable the estimation of a model's equilibrium climate sensitivity (Zelinka et al., 2020). Its protocol remains unchanged as in the CMIP5, facilitating comparisons across CMIP generations.

The *lgm* experiment is designed to examine the effect of altered ice sheets, continental extent due to reduction in sea level, and lower GHG forcings (Kageyama et al., 2018). The concentrations of CO<sub>2</sub>, NH<sub>4</sub> and N<sub>2</sub>O are set to 190 ppm, 375 ppb and 200 ppb, respectively, in the PMIP4, and 185 ppm, 350 ppb and 200 ppb in the PMIP3. The major difference between the PMIP3 and PMIP4 *lgm* simulations is the choice of the prescribed ice sheets. While the PMIP3 simulations all used the same composite ice-sheet reconstructions (Abe-Ouchi et al., 2015), the PMIP4 simulations chose one of the three as summarised in Kageyama et al. (2021): the original PMIP3-CMIP5 ice sheet (Abe-Ouchi et al., 2015), GLAC-1D (Ivanovic et al., 2016) and ICE-6G\_C (Peltier et al., 2015; Argus et al., 2014). Although these reconstructions have similar ice sheet extent, they differ in the heights of the Laurentide, Fennoscandian, and West Antarctica Ice Sheet.

The *midHolocene* and *lig127k* experiments are designed to examine the climate system responses to orbital forcings that differ from the PI (Kageyama et al., 2018). The experimental designs for the two experiments are outlined by Otto-Bliesner et al. (2017). In the PMIP4, the concentrations of CO<sub>2</sub>, NH<sub>4</sub> and N<sub>2</sub>O in the *midHolocene* experiment are set to 264.4 ppm, 597 ppb and 262 ppb, respectively, while those

**Table 1.** Models contributing to the control experiment (*piControl*), the PMIP experiments (*midHolocene* (MH); *lig127k* (LIG); *lgm* (LGM)) and an idealised CO<sub>2</sub> experiment (*abrupt4xCO2* (4xCO<sub>2</sub>)) under the CMIP5 and the CMIP6. Numbers in column Participation represent the length of model years of each simulation.

| Model           | PMIP | ECS*<br>(K) | Participation |     |     |     | REF.                          |
|-----------------|------|-------------|---------------|-----|-----|-----|-------------------------------|
|                 |      |             | PI            | MH  | LIG | LGM |                               |
| AWI-ESM-1-1-LR  | 4    | 3.6         | 100           | 100 | 100 | 100 | Sidorenko et al. (2015)       |
| BCC-CSM1-1      | 3    | 3.1         | 500           | 100 |     |     | 50<br>Xin et al. (2013)       |
| CCSM4           | 3    | 2.9         | 1051          | 301 |     | 101 | 50<br>Gent et al. (2011)      |
| CESM2           | 4    | 5.3         | 500           | 700 |     |     | 50<br>Gettelman et al. (2019) |
| CNRM-CM5        | 3    | 3.3         | 850           | 200 |     | 200 | 50<br>Voldoire et al. (2013)  |
| CNRM-CM6-1      | 4    | 5.1         | 500           |     | 301 |     | 50<br>Voldoire et al. (2019)  |
| COSMOS-ASO      | 3    |             | 399           |     |     | 600 | Budich et al. (2010)          |
| CSIRO-Mk3-6-0   | 3    | 4.1         | 500           | 100 |     |     | 50<br>Rotstayn et al. (2011)  |
| CSIRO-Mk3L-1-2  | 3    | 3.1         | 1000          | 500 |     |     | Phipps et al. (2012)          |
| EC-EARTH-2-2    | 3    | 4.2         | 40            | 40  |     |     | Hazeleger et al. (2012)       |
| EC-Earth3-LR    | 4    | 4.3         | 201           | 203 | 210 |     | Döscher et al. (2022)         |
| FGOALS-f3-L     | 4    | 3           | 561           | 500 | 500 |     | 50<br>He et al. (2020)        |
| FGOALS-g2       | 3    | 3.7         | 700           | 680 |     | 100 | 50<br>Li et al. (2013)        |
| FGOALS-g3       | 4    | 2.9         | 700           | 500 | 500 |     | Li et al. (2020)              |
| FGOALS-s2       | 3    | 4.5         | 501           | 100 |     |     | 50<br>Bao et al. (2013)       |
| GISS-E2-1-G     | 4    | 2.7         | 851           | 100 | 100 |     | 50<br>Kelley et al. (2020)    |
| GISS-E2-R       | 3    | 2.1         | 500           | 100 |     | 100 | 50<br>Schmidt et al. (2014)   |
| HadGEM2-CC      | 3    | 4.5         | 240           | 35  |     |     | Collins et al. (2011)         |
| HadGEM2-ES      | 3    | 4.6         | 336           | 101 |     |     | 50<br>Collins et al. (2011)   |
| HadGEM3-GC31-LL | 4    | 5.4         | 100           | 100 | 200 |     | Williams et al. (2018)        |
| INM-CM4-8       | 4    | 2.1         | 531           | 200 | 100 | 200 | 50<br>Volodin et al. (2018)   |
| IPSL-CM5A-LR    | 3    | 4.1         | 1000          | 500 |     | 200 | 50<br>Dufresne et al. (2013)  |
| IPSL-CM6A-LR    | 4    | 4.5         | 1200          | 550 | 550 |     | 50<br>Boucher et al. (2020)   |
| KCM1-2-2        | 3    |             | 200           | 100 |     |     | Park et al. (2009)            |
| MIROC-ES2L      | 4    | 2.7         | 500           | 100 | 100 | 100 | 50<br>Hajima et al. (2020)    |
| MIROC-ESM       | 3    | 4.7         | 630           | 100 |     | 100 | 50<br>Sueyoshi et al. (2013)  |
| MPI-ESM-P       | 3    | 3.5         | 1156          | 100 |     | 100 | 50<br>Giorgetta et al. (2013) |
| MPI-ESM1-2-LR   | 4    | 2.8         | 1000          | 500 | 300 |     | 50<br>Mauritsen et al. (2019) |
| MRI-CGCM3       | 3    | 2.6         | 500           | 100 |     | 100 | 50<br>Yukimoto et al. (2012)  |
| MRI-ESM2-0      | 4    | 3.1         | 701           | 200 |     |     | 50<br>Yukimoto et al. (2019)  |
| NESM3           | 4    | 3.7         | 100           | 100 | 100 |     | 50<br>Cao et al. (2018)       |
| NorESM1-F       | 4    | 2.3         | 200           | 200 | 200 |     | Guo et al. (2019)             |
| NorESM2-LM      | 4    | 2.5         | 391           | 100 | 100 |     | 50<br>Seland et al. (2020)    |
| UoF-CCSM-4      | 4    | 3.2         | 100           | 100 |     | 100 | Peltier and Vettoretti (2014) |
| Ensemble size   |      |             | 34            | 32  | 14  | 13  | 23                            |

\* No values for the ECS of COSMOS-ASO and KCM1-2-2 were found.

in the *lig127k* experiment are set to 275 ppm, 685 ppb and 255 ppb, respectively. The *midHolocene*, included since the beginning of the PMIP (Joussaume and Taylor, 1995; Brannon et al., 2000), set to an orbital configuration at 6 ka following Berger (1978) and Berger and Loutre (1991). The orbit at 6 ka was characterised by larger obliquity, and its perihelion occurred near the boreal autumn equinox. The prescribed GHG concentrations in the PMIP4 *midHolocene* use more realistic concentrations derived from ice cores and observations (Otto-Bliesner et al., 2017) than the PMIP3, which contributes to a decrease of  $0.3 \text{ W m}^{-2}$  in effective radiative forcing (Otto-Bliesner et al., 2017). The concentrations

of CO<sub>2</sub>, NH<sub>4</sub> and N<sub>2</sub>O in the PMIP3 *midHolocene* experiment are set to 280 ppm, 650 ppb and 270 ppb, respectively. The *lig127k* uses the orbital configuration at 127 ka (Berger and Loutre, 1991), characterised by a larger eccentricity than the PI and its perihelion close to the boreal summer solstice. Both periods were characterised by receiving more insolation at the top of the atmosphere (TOA) in the Northern Hemisphere during June–July–August (JJA) and less incoming solar radiation in both hemispheres during DJF compared to 1850 CE, with the LIG having stronger orbital forcing than the MH.

### 2.3 Analysis and definitions

The analysis in this work follows the workflow described by Zhao et al. (2022). We create a curated replica of the relevant simulation outputs available on the System Grid Federation (ESGF; Balaji et al., 2018), which stores the CMIP6 outputs in a standardised format (Juckes et al., 2020). Digital Object Identifier (doi) for each simulation downloaded from the ESGF can be found in the Supplement. We also require some simulations from the model groups if they are not available on the ESGF. Then we apply calendar adjustment on the *midHolocene*, *lig127k* and *lgm* monthly output that re-aggregate the monthly output from a present-day calendar to those representing the past via the PaleoCalAdjust software by Bartlein and Shafer (2019).

The PMIP simulations do not have a fixed length. The length depends on when the simulations meet the criteria: (a) the absolute trend in global mean sea surface temperature is less than 0.05 K per century, and (b) the Atlantic meridional overturning circulation (AMOC) is stable (Kageyama et al., 2018). For the *piControl* experiment, CMIP6 requires a minimum of 500 years to ensure an equilibrium state (Eyring et al., 2016). For these equilibrium simulations, we take the average of the simulations (see Table 1 for the length of model years of each simulation). The CMIP protocol specifies a minimum length of 150 years for the *abrupt4xCO2* simulations (Eyring et al., 2016). For consistency in our analysis, we take the last 50 years of the *abrupt4xCO2* simulations for a direct comparison with other simulations employed in this study.

The Climate Variability Diagnostics Package (CVDP; Brierley and Wainer, 2018) had been modified for palaeoclimate purposes (Brierley and Wainer, 2018). We run the modified CVDP on each simulation to calculate multiple pertinent time series and spatial fields. The CVDP outputs have been regridded to  $1^\circ$  by  $1^\circ$  before analysing to eliminate the effects of different native resolutions across all the models. Multi-model mean anomalies take the average of regridded anomaly (*experiment* – *piControl*) across the ensemble members (Brierley and Wainer, 2018). Please see Zhao et al. (2022) for more details. We evaluate ensemble consistency via the threshold at which at least two-thirds of the models agree on the sign of the multi-model mean. Results of the PMIP4 and PMIP3 have not shown fundamental differences in statistics (Brierley et al., 2020; Kageyama et al., 2021), so we, therefore, combine the two indistinguishable phases in the purpose to enlarge the size of ensembles, which have been adopted in analysing ENSO (Brown et al., 2020) and Indian dipole (Brierley et al., 2023) across experiments.

Here, we adopt the definition of NAO as the leading EOF of DJF SLP anomalies over the Northern Hemisphere north of  $20^\circ$  to  $80^\circ$  N and  $90^\circ$  W to  $40^\circ$  E (hereafter referred to as the NAO pattern). The NAO index is the normalised PC time series of the EOF. Instead of using the NAO index, we use the amplitude of NAO to show its strength, which is mea-

sured as the standard deviation of the renormalised PC time series (i.e. the NAO index times the standard deviation of the spatial NAO pattern over the region). We also present spatial patterns associated with the NAO by linearly regressing the monthly temperature and precipitation onto the NAO index to evaluate the association between the NAO and surface climate variables (Brierley and Wainer, 2018). We also examine the similarity between the NAO and the Northern Annular Mode (NAM) in the PMIP experiments. All the experiments show that NAM and NAO are strongly correlated in the time series of the NAO indices, explained by variance and amplitude (not shown). Therefore, the following sections do not distinguish the NAO from the NAM.

### 3 Comparison with observations

Before looking at the response in experiments, we first evaluate the ability of the CMIP models used in this study to reproduce the North Atlantic climate states during the PI by comparing the *piControl* simulations with the C20 Reanalysis dataset (Compo et al., 2011), as shown in Fig. 1. Models generally capture the spatial pattern of observed mean DJF surface air temperature (SAT), but are biased in producing too cold Arctic, especially over Greenland and Nunavut (Fig. 1a, b). The cold bias has been detected by earlier PMIP analyses on a single experiment (Brierley et al., 2020; Otto-Bliesner et al., 2021), both showing a large spread across the models in Arctic regions between  $60^\circ$  and  $90^\circ$  N. The bias is partly associated with the model's representation of cloud radiative processes (Zhang et al., 2023) and atmospheric dynamics (Hall et al., 2021) and may also be affected by Arctic hydrography (Khosravi et al., 2022). Figure 1c and d show that models capture the DJF mean precipitation pattern over the North Atlantic Ocean, though they underestimate the amount of precipitation and shift the maximum location westward slightly as compared to the observation. The simulated SLP generally agrees with the observation (Fig. 1e, f), although it produces lower pressure along the coast of Greenland.

The NAO is the leading EOF of DJF SLP over the North Atlantic-Europe sector, showing a dipole structure with the negative anomaly over the northern centre and the positive anomaly over the southern centre (see Sect. 2.3). The *piControl* simulations show a distinguishable positive phase with a strong negative SLP centre over the northeast of Iceland and a positive centre over the northeast of the Azores (Fig. 1g, h). The simulated pattern shows such a dipole structure during the PI, which is consistent with observations, but the simulated negative anomalies extend further into the centre of Greenland, and the positive anomalies around  $30^\circ$ – $40^\circ$  N North Atlantic Ocean are underestimated. Notably, 9 out of the 34 models display an eastward shifted positive centre over Europe along with varying degrees of pattern strength, and one model produces dipole positive centres over the Mediterranean and the central USA (not shown). In the *pi-*

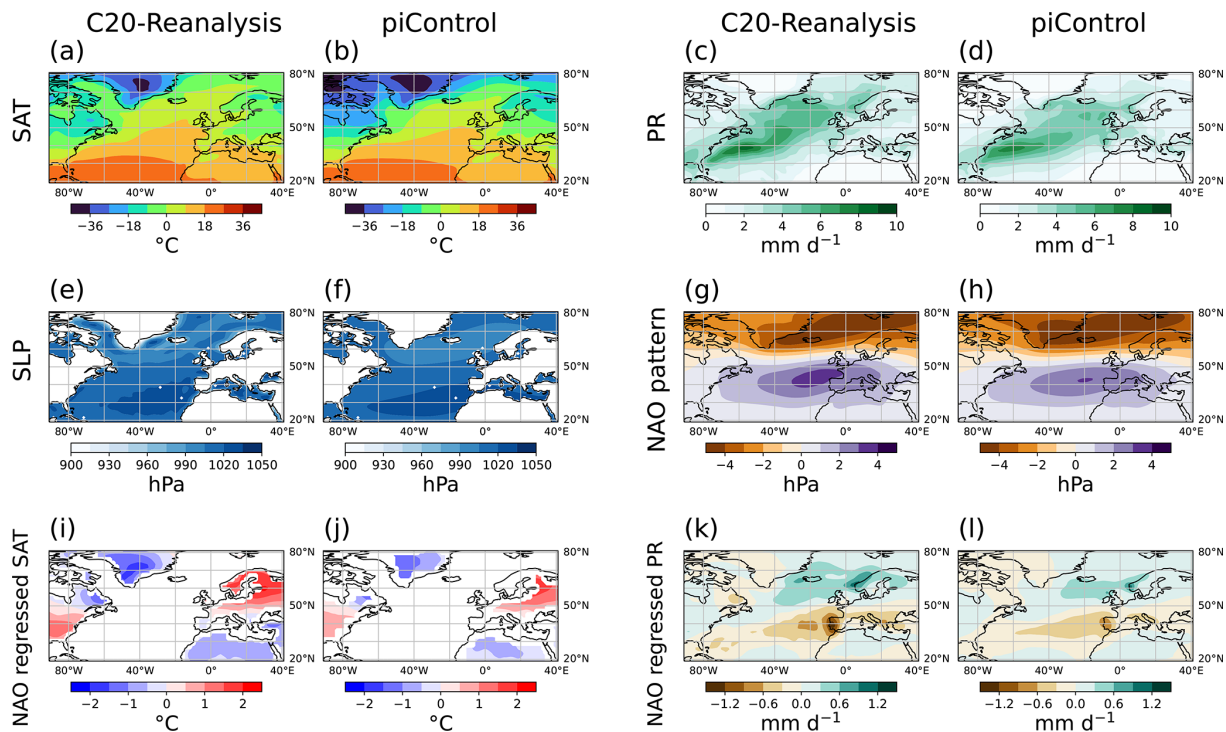


**Figure 1.** Comparison between observations taken from the 20th-Century Reanalysis (Compo et al., 2011) and the multi-model mean of the *piControl* simulations. Panels show DJF mean variables over the North Atlantic sector (see Sect. 2.3 for region definition). Panels present the (a, b) surface air temperatures in °C (SAT), (c, d) precipitation in  $\text{mm d}^{-1}$  (PR), (e, f) sea level pressure in hPa (SLP), (g, h) NAO pattern in hPa, and teleconnections between NAO and (i, j) SAT in °C and (k, l) PR in  $\text{mm d}^{-1}$  computed by regression against the NAO.

*Control* simulations, the NAO accounts for 41.5 % of the total variance (34.3 %–52.0 %; corresponding to the PI explained variance shown by the vertical range of black dots in Fig. 2a and the horizontal range of dots in Fig. 2b), slightly less than the 42.3 % observed in observational data (pink dashed lines in Fig. 2).

The *piControl* SAT imprint of the NAO shows a pattern of warmer mid-latitudes and colder subpolar and subtropical regions than the observation (Fig. 1i, j), with the effect of a stronger jet stream located further north, stronger trade winds and northward shift of extratropical storms associated with a positive phase of NAO (IPCC, 2021b). The related northward shift of storm tracks with positive NAO phases results in a wetter northern Europe, a drier southern Europe and a northward shift of precipitation over the ocean. Both observations and models capture the pattern (Fig. 1k, l), but the simulated pattern is smoother than the observation with underestimated change magnitudes.

#### 4 Change in mean state

Both the MH and the LIG were characterised by receiving less incoming solar radiation globally during DJF compared to 1850 CE, with a stronger reduction at 127 ka, suggesting an expectation of cooling in both experiments. The merid-

ional SAT gradients of the *midHolocene* and *lig127k* experiments are weaker than the *piControl*, and the *lig127k* displays a stronger signal (Fig. 3a, d). The DJF mean temperature change averaged over the North Atlantic sector in the *midHolocene* experiment is  $0.07^\circ\text{C}$  cooler than the *piControl*. The cooling is stronger in the *lig127k* experiment at  $-0.52^\circ\text{C}$ . Both experiments produce polar amplification, though the signal is inconsistent across the ensembles. The *lig127k* simulations show a large spread across the models in producing Arctic warming, and the *midHolocene* simulations show a larger ensemble spread over the whole region of the North Atlantic sector (Fig. 3a, d). The Euro-Atlantic precipitation fields show a drier Europe and an apparent drying off of the North American east coast in both experiments as compared to the *piControl* (Fig. 3b, e). There is a wetting over the rest of the Atlantic in the ensemble average, although the models do not all agree on the sign of the change. The signal of multi-model mean precipitation change is affected by NorESM2-LM, which produces a much larger precipitation increase north of  $40^\circ\text{N}$  than other models in both experiments. Figure 3c, f shows that SLP increases over lower latitudes and decreases over high latitudes.

The Arctic warming during the boreal winter suggests other important processes, e.g., polar amplification with smaller and thinner sea ice in the Arctic (Serreze and Barry,

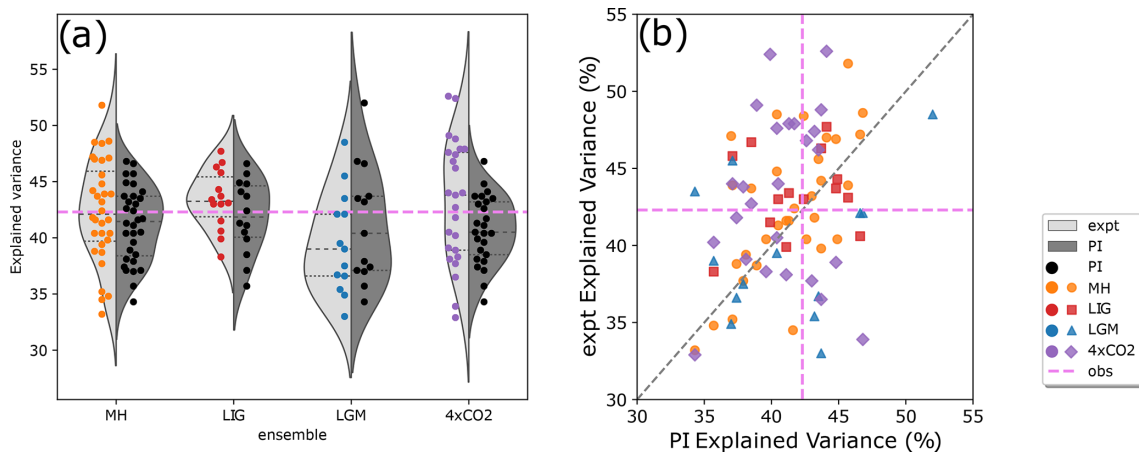


**Figure 2.** Total variance (%) explained by the NAO for (a) the experiments and (b) the models. Experimental names are abbreviated to MH for the *midHolocene*, LIG for the *lig127k*, LGM for the *lgm*, 4xCO2 for the *abrupt4xCO2*, and PI for the *piControl*, respectively. (a) For each column, the dots (corresponding to the left y-axis) show the explained variance by models. The distributions are computed via a kernel density estimation (Waskom, 2021): The curves and shading show the distributions of the explained variance by models for each experiment (left, shading in light grey) and the corresponding *piControl* (right, shading in dark grey); horizontal black dashed and dotted lines within each curve represent the median and 75 % and 25 % quartiles, respectively; pink dashed line across the panel represents the explained variance from the observation. The horizontal location of dots within each column has been offset for better visibility. (b) Each dot shows the comparison of the explained variance between the experimental simulation and the *piControl* by the model; pink dashed lines represent the explained variance from the observation.

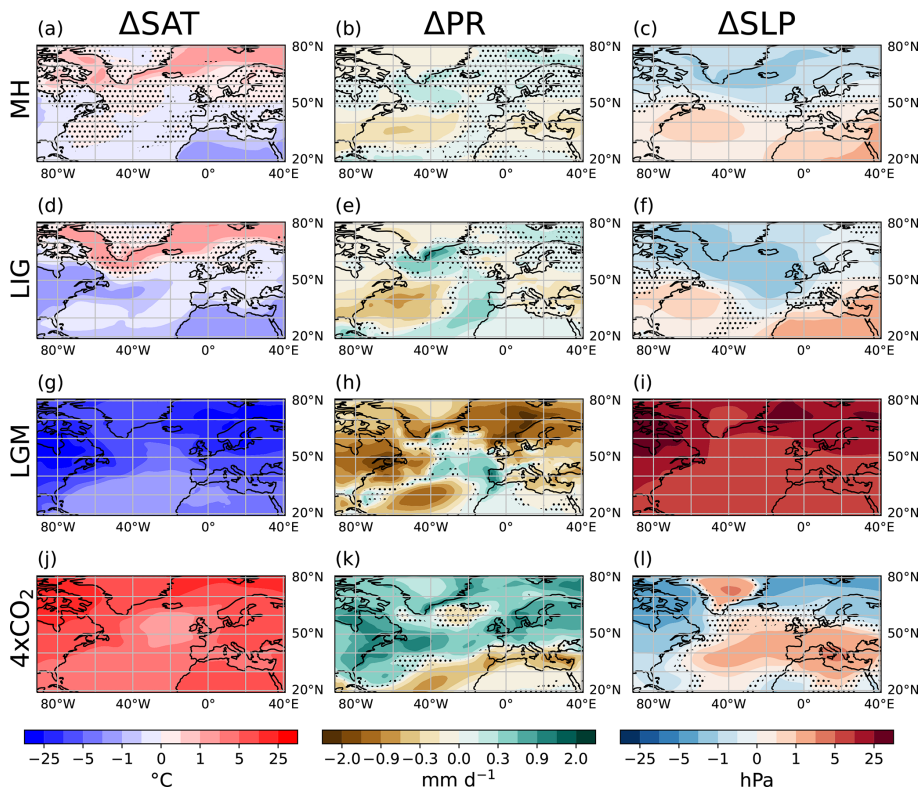


**Figure 3.** Multi-model mean change in mean states between experiments and the *piControl*. The columns from left to right show the DJF mean surface air temperature in °C (SAT; a, d, g, j), precipitation in mm d<sup>-1</sup> (PR; b, e, h, k), and sea level pressure in hPa (SLP; c, f, i, l). The rows from top to bottom represent the ensemble mean difference for the (a, b, c) *midHolocene* (MH), *lig127k* (LIG; d, e, f), *lgm* (LGM; g, h, i), and *abrupt4xCO2* (4xCO2; j, k, l) experiments. Stippling indicates where the ensemble is inconsistent in the direction of change, i.e., at least two-thirds of the models disagree on the sign of the multi-model mean.

2011) and ocean memory (Marino et al., 2015; Govin et al., 2012). Meanwhile, neither of the two experiments (*mid-Holocene* and *lig127k*) incorporates some regional processes that can cause regional coolings. For example, the *lig127k* simulations did not include meltwater from ice sheets over Scandinavia and Canada related to the cooling in the Nordic Seas and south of Greenland shown by LIG reconstruction (Barlow et al., 2018; Otto-Bliesner et al., 2021). Earlier studies have compared the experiments with reconstructions and have confirmed that both experiments underestimate the Arctic warming (Brierley et al., 2020; Otto-Bliesner et al., 2021). The underestimated MH Arctic warming has existed since the PMIP3-CMIP5 (Harrison et al., 2015; Yoshimori and Suzuki, 2019). The regional temperature bias in the CMIP5 *midHolocene*, *piControl* and *historical* are similar (Ackerley et al., 2017; Harrison et al., 2015), which indicates the persistent errors in representing the climate system.

The LGM was characterised by a colder climate with a global mean cooling of 5–7 °C (Gulev et al., 2021) and large ice sheets covering the mid- to high-latitudes in the Northern Hemisphere (Clark and Mix, 2002; Clark et al., 2009). The averaged DJF cooling over the North Atlantic sector is –9.86 °C in the *lgm* simulations compared to the *piControl*. The *lgm* simulations show consistent cooling over the sector with a greater temperature decrease over land than over sea (Fig. 3g). The greatest cooling is found over the Norwegian and Barents Seas and parts of Scandinavia and North America, which reflects the change in surface height and albedo related to ice sheet change (Kageyama et al., 2021). The cooling is also partly affected by the advection of the cold temperature anomalies downwind of the ice sheets (Kageyama et al., 2021) and is partly related to a weakened AMOC (Jonkers et al., 2023). Though the cooling signal is consistent, the ensemble shows a large spread in simulating the magnitude of cooling affected by the choice of ice sheets of the PMIP3 simulations shown in Kageyama et al. (2021). Shi et al. (2023) decomposed the contributions of individual boundary conditions and forcings to the LGM cooling, finding that the cooling over the sea within the region is mainly due to the GHG forcings, and cooling over the continent is caused by changes in ice sheets. The *lgm* simulations show enhanced precipitation over the mid-latitudes of the North Atlantic Ocean as compared to the *piControl*, but the signal is not consistent across the ensemble (Fig. 3h). The SLP increases uniformly in the *lgm* simulations (Fig. 3i), consistent with the enhanced SAT cooling (Fig. 3g). The higher SLP over the polar regions, coupled with a cooler and drier climate, is related to the large Laurentide Ice Sheet (Otto-Bliesner et al., 2006).

The *abrupt4xCO2* simulations contrast with the *lgm*, showing consistent warming across the whole North Atlantic region, with greater warming over land (Fig. 3j), amounting to 6.4 °C over the sector. The weakest warming appears over the ocean south of Iceland, where the surface current of the AMOC densifies and sinks to form deep water. Earlier stud-

ies suggest the AMOC weakening in the *abrupt4xCO2* experiment in response to warming (Zhu et al., 2023; Madan et al., 2024). The switch of precipitation change signal represents a northward shift of the jet stream (Fig. 3k) relative to the *piControl*, whereas the inconsistency shows the uncertainty in producing the location of the jet stream, arising from both model bias and internal variability. Though the increase in the multi-model mean of *abrupt4xCO2* precipitation change is consistent (Fig. 3k), the spatial pattern of the change by individual models is complex (not shown). The weakened precipitation south of Iceland is inconsistent across the *abrupt4xCO2* ensemble (Fig. 3k), as about half of the models produce such a reduction. The pattern of *abrupt4xCO2* SLP change (Fig. 3l) is not consistent with temperature change. The inactive prescribed Greenland Ice Sheet in simulations (Eyring et al., 2016) causes the SLP to increase over the region.

## 5 Change in NAO

The NAO patterns of the two orbital experiments (*mid-Holocene* and *lig127k*) are not distinguishable from the *piControl* (Fig. 4a, c). The similarity in the NAO pattern between the *midHolocene* and the *piControl* agrees with the findings of earlier modelling studies (Otto-Bliesner et al., 2006; Gladstone et al., 2005; Stephenson et al., 2006). It is also consistent with the PMIP2 simulations (Lü et al., 2010) that found the MH leading EOF of DJF SLP is similar to the PI. Models produce complex changes in the NAO pattern in both experiments and show a spread south of Greenland and Iceland near 50° N (Fig. 4b, d). Of the 32 models, 11 display a clear weakened, and 7 show an enhanced positive NAO phase in the *midHolocene*, respectively, as compared to the *piControl*; a similar result of spatial change occurs for the *lig127k* experiment, as 6 (5) out of the 14 models display weakness (enhancement) in the *lig127k* as compared to the *piControl* (not shown).

The average percentage of explained variance during the *midHolocene* is 42.4 % (33.2 %–51.8 %), whose range is close to the *piControl* (Fig. 2a). The absence of clear changes in explained variance between *midHolocene* and *piControl* is consistent with Gladstone et al. (2005), which, in conjunction with inter-model inconsistencies, leads to uncertainties about the MH NAO behaviour. Changes in explained variance vary across the ensemble (Fig. 2b), ranging from –7.1 % to 10.1 %. In the *lig127k* simulations, models display an averaged explained variance at 43.4 % (38.3 % to 47.7 %), different from the 42.7 % (35.7 %–52.0 %) in the corresponding *piControl* simulations (Fig. 2a). Changes in explained variance by individual models vary across the ensemble and do not show a trend (Fig. 2b).

Figure 5 shows that the NAO amplitude in the *mid-Holocene* simulations is 2.31 hPa (0.77–3.15 hPa). The range and distribution of the *midHolocene* NAO amplitude is sim-

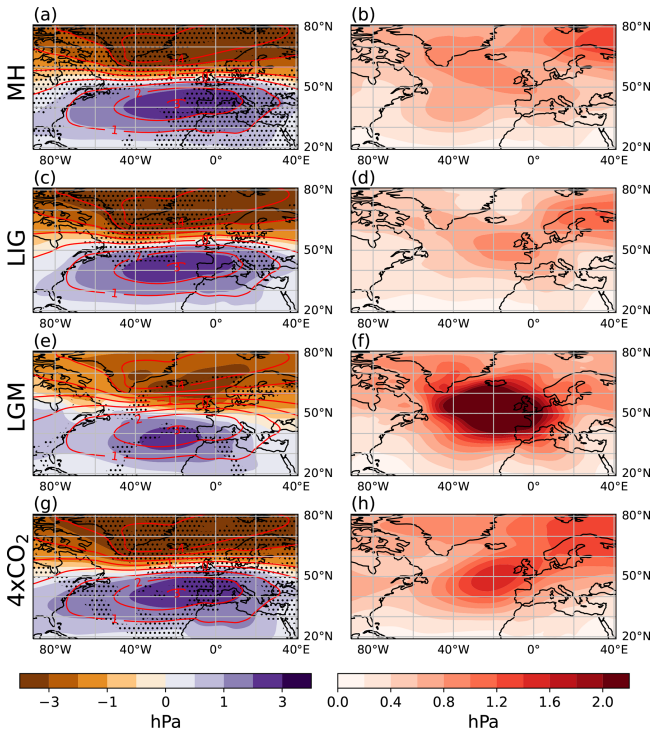


**Figure 4.** Multi-model mean DJF SLP spatial pattern for NAO (hPa) in each experiment (shadings, left column) and ensemble variation (right column), including the *midHolocene* (MH; a), *lig127k* (LIG; c), *lgm* (LGM; e) and *abrupt4xCO2* (4xCO<sub>2</sub>; g). Red contours represent the pattern of the *piControl*, and stippling indicates where the ensemble is inconsistent in the direction of change. Ensemble variation is presented as the standard deviation across the ensemble (b, d, f, h).

ilar to those of the *piControl* (Fig. 5), though the differences between *midHolocene* and *piControl* by individual models range from  $-0.30$  to  $0.79$  hPa. Though 19 out of 32 models present increased NAO amplitude, the ensemble mean change in the NAO amplitude is  $0.06$  hPa (Fig. 5). The slight increase is largely affected by 3 models, which contribute an intensification at  $0.79$ ,  $0.50$  and  $0.43$  hPa, respectively. The *lig127k* NAO amplitude is  $2.18$  hPa, similar to the *piControl* at  $2.28$  hPa with a more concentrated distribution (Fig. 5). The results of the two orbital-driven experiments suggest that the NAO response is unaffected by the seasonal variation induced by altered orbital configurations.

In the *lgm* experiment, the NAO is weaker as compared to the *piControl* (Fig. 4e). There is a southward shift of both the negative and positive centres of the NAO as compared to the *piControl* (Fig. 4e), though with a large model spread over the N. Atlantic Ocean between  $40$  and  $65^\circ$  N (Fig. 4f). The weakened NAO and centre shifts in the *lgm* are consistent with the results of Lü et al. (2010) and Otto-Bliesner et al. (2006). Models show large variations in producing the location of positive and negative centres of the NAO. 8 out of the 13 models display the switch of signal between  $50$

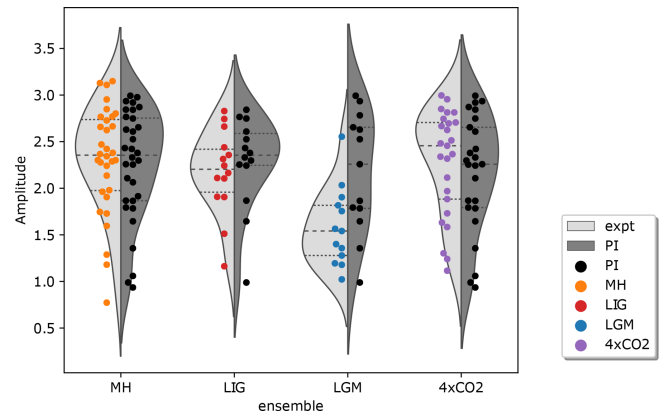


**Figure 5.** Same as Fig. 2a but for the NAO amplitude (hPa) for the experiments. The amplitude is measured as the standard deviation of the renormalised NAO PC time series (Sect. 2.3).

and  $60^\circ$  N, where a model displays its negative centre while another model shows its positive centre (not shown). The NAO explains  $39.6\%$  ( $33\%$ – $48.5\%$ ) of SLP variability in the *lgm* that is  $-1.6\%$  less than the corresponding *piControl* simulations (Fig. 2a). The majority of the models show a reduction in explained variance (Fig. 2b), except three models show enhancements at  $9.2\%$ ,  $8.7\%$  and  $3.3\%$ . The *lgm* NAO amplitude is  $1.58$  ( $1.02$ – $2.55$ ) hPa, which is  $0.59$  hPa weaker than the *piControl* (Fig. 5), and one model contributes to the largest reduction in amplitude at  $-1.61$  hPa. Only three models contribute to enhanced amplitude in the *lgm* simulations. Quartiles and median in Fig. 5 show a general reduction in *lgm* amplitude with respect to the *piControl*, which implies a weaker NAO in the *lgm*. The reduction is partly related to the presence of the Laurentide and Scandinavian Ice Sheets (Braconnot et al., 2007). Justino and Peltier (2005) suggested that these two ice sheets induce changes in the stationary waves, sea-ice extent and the oceanic meridional overturning circulation, which provides key context for the LGM NAO responses in this study.

The *abrupt4xCO2* experiment shows the opposite change in the NAO pattern by showing enhancement and a slight northward shift in centres than the *piControl* (Fig. 4g, h). Models produce increased explained variance (Fig. 2) and stronger amplitude (Fig. 5) than the *piControl*. The *abrupt4xCO2* simulations explain  $43.2\%$  ( $32.9\%$ – $52.6\%$ ) of the SLP anomalies, which are  $2.4\%$  ( $-12.9\%$  to  $12.5\%$ ) larger than the corresponding *piControl* simulations. Only 6 out of 25 models produce a reduction in explained variance, in which one model presents the largest reduction by  $-12.9\%$ , even larger than that in the *lgm* simulation at  $-4.7\%$  as compared to the *piControl*. The NAO amplitude in the *abrupt4xCO2* experiment is  $2.28$  hPa on average (ranging from  $1.12$  to  $3.00$  hPa). Though the mean NAO amplitude of the *abrupt4xCO2* is  $0.11$  hPa higher than the corresponding *piControl*, the median of *abrupt4xCO2* NAO amplitude

is slightly lower than that of the corresponding *piControl* (Fig. 5). Overall, the NAO is sensitive to GHG forcing and temperature change, as the warming strengthens the NAO, which implies that GHG changes in the future might play a role in modulating NAO behaviour.

As described in Sect. 1, the NAO variability is primarily driven by the internal variability of mid-latitude atmospheric dynamics (Lorenz and Hartmann, 2003). The findings of Rind et al. (2005a, b) show that both tropospheric and stratospheric climate changes influence the NAO response via altering propagating waves, angular momentum transport, and planetary wave energy. SST (Mosedale et al., 2006; Hurrell et al., 2004), GHG forcing (Stephenson et al., 2006; Barnes and Polvani, 2013), sea ice (Pedersen et al., 2016; Smith et al., 2017) and snow cover changes (Henderson et al., 2018; Spencer and Essery, 2016) could also be potential drivers. Rind et al. (2005b) stated that the Arctic Oscillation response during the Ice Age was dominated by changes in the eddy transport of sensible heat and local high-latitude forcing. Lü et al. (2010) examined the drivers of the NAO variability in the PMIP2 *midHolocene* and *lgm* experiments and found that the upward-propagating stationary Rossby waves might lead to NAO amplitude weakening. Based on four simulations, their *midHolocene* experiment presented a slight reduction in the Arctic Oscillation intensity. Our results show the opposite change as the NAO amplitude is slightly strengthened, but this finding is affected by a few models that produce a large enhancement. Our results of the *lgm* and *abrupt4xCO2* experiments agree with the findings of Rind et al. (2005a, b), as the NAO increases under warmer states and decreases under colder states. They stated that the NAO index change is related to the eddy angular momentum transport change. The weakened *lgm* NAO amplitude is possibly due to cooler SST and reduced atmospheric moisture content as well as a shift of stationary waves and a weakened polar vortex linked to wave-mean flow interaction, and thus a reduction in polar westerlies (Lü et al., 2010). The internal variability is less important in contributing to model spread in this study, as the results are averaged over substantially longer periods (Sect. 2). The large model spread here is mainly attributed to the differences in model structure (McKenna and Maycock, 2021).

## 6 Associated Changes in the Climate Teleconnections

A positive NAO in the *piControl* is associated with warmer and wetter northern Europe and central North America and colder and drier Mediterranean and northern North America (Fig. 1j, l). Compared with the *piControl*, the *midHolocene* experiment shows a warmer continent associated with the NAO (Fig. 6a), with the warming extending farther into central Eurasia and central North America (not shown). Differently, the *lig127k* shows cooler conditions over north-

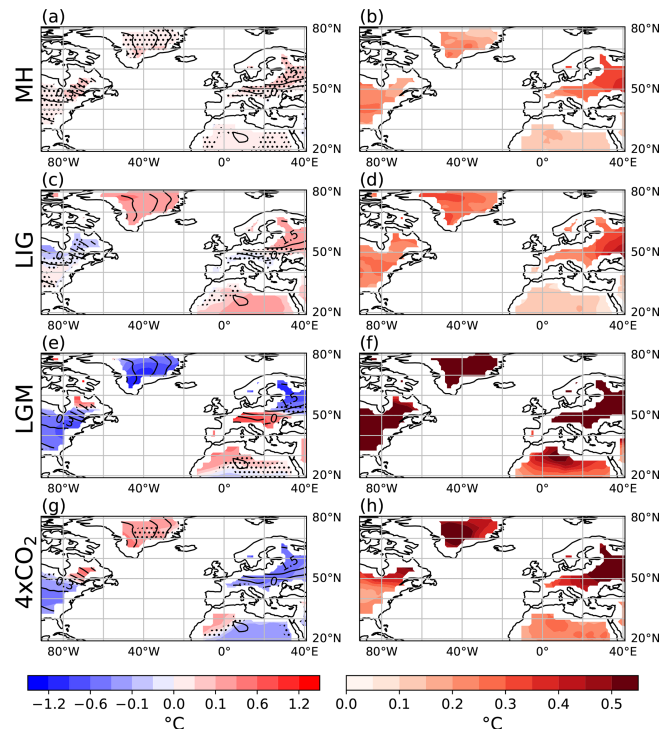


**Figure 6.** Multi-model mean change in DJF surface air temperature ( $^{\circ}\text{C}$ ) associated with the NAO as compared to the *piControl* (shadings, left column) and ensemble variation (right column). Experiments include *midHolocene* (MH; a), *lig127k* (LIG; c), *lgm* (LGM; e) and *abrupt4xCO2* ( $4x\text{CO}_2$ ; g). Black contours show the pattern of the *piControl*. Stippling indicates where the ensemble is inconsistent in the direction of change. Ensemble variation is presented as the standard deviation across the ensemble (b, d, f, h).

ern North America and central Europe than the *piControl* (Fig. 6c). The DJF mean precipitation associated with the NAO increases over the North Atlantic Ocean north of  $30^{\circ}\text{N}$  and over northern Europe, while it decreases over central Europe and North America in the *midHolocene* (Fig. 7a). The *lig127k* experiment shows a similar pattern but with less precipitation over east of  $20^{\circ}\text{W}$  and north of  $50^{\circ}\text{N}$  relative to the *piControl* (Fig. 7c). However, mean changes in the DJF mean temperature and precipitation associated with the NAO are not robust in the *midHolocene* and *lig127k* as compared to the *piControl*, and the changes are not consistent across the ensembles (Figs. 6a–d and 7a–d). The MH models capture changes in the mean state (Fig. 3a) that project onto the positive phase of the NAO (Fig. 1h), as reconstructed by Funder et al. (2011). Proxy reconstructions also suggest that regional temperature patterns over Europe were primarily forced by a positive NAO-like phase during the MH as opposed to radiative responses forced by changes in the seasonal insolation cycle (Rimbu et al., 2003; Mauri et al., 2014). However, none of these papers include archives with sufficiently high temporal resolution to compare with the inter-annual variability being investigated here.

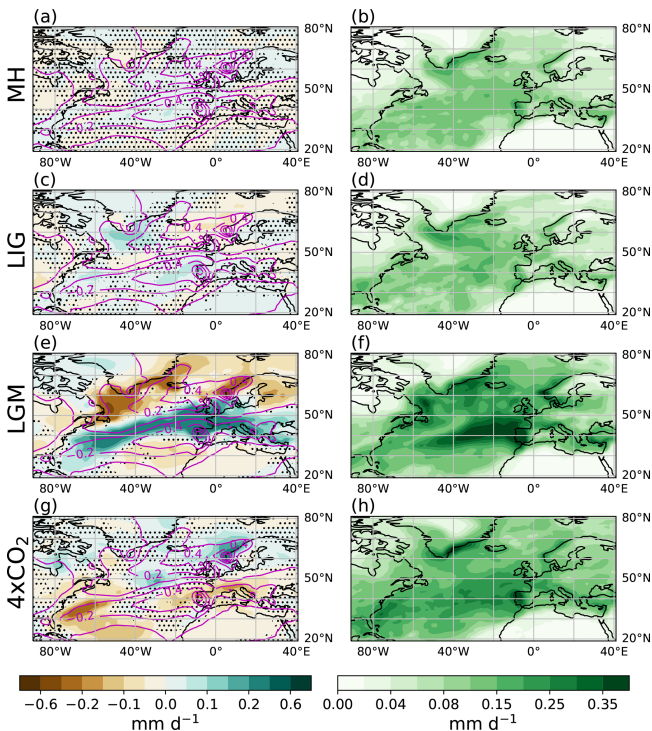


**Figure 7.** Same as Fig. 6 but for multi-model mean change in DJF precipitation ( $\text{mm d}^{-1}$ ) associated with the NAO. Magenta contours show the pattern of the *piControl*. Stippling indicates where the ensemble is inconsistent in the direction of change.

The temperature and precipitation patterns associated with the NAO shift southward in the *lgm* experiment (Figs. 6e and 7e), which suggests a reduction of features of the positive boreal winter NAO. Associated with the NAO, the *lgm* experiment presents colder and drier central North America and northern Europe and warmer and wetter Mediterranean and northern North America than the *piControl*, with the patterns extending to central continents (not shown). As the strengthened precipitation teleconnection pattern over the western Iberian Peninsula is also present in the mean-state change (Fig. 3h), it suggests that the strengthened Mediterranean precipitation pattern is not necessarily directly forced by the NAO. In the *abrupt4xCO2* experiment, opposite to the *lgm*, features of the positive boreal winter NAO are enhanced compared to the *piControl* (Figs. 6g and 7g). The associated changes in temperature and precipitation do not match the pattern and magnitude of robust change in mean state temperature and precipitation (Fig. 3), which implies that changes have less influence on change in mean state climatology in the NAO and have other attributions. For example, the large ice sheets during the LGM limited turbulent air-sea heat fluxes in the high-latitude North Atlantic that influenced the NAO and cooled the temperature (Sect. 4). The warming in the *abrupt4xCO2* can be explained by the thermodynamic processes affecting heat and moisture transport

without changing the large-scale atmospheric circulation patterns (Stephenson et al., 2006). The enhanced warming of the surface boundary layer enhances vertical latent heating, which in turn influences the atmospheric moisture content and baroclinic stability (Lorenz and DeWeaver, 2007).

NAO greatly impacts the European climate (Sect. 1). Figure 8 shows the relationships between the changes in NAO amplitude and changes in DJF mean precipitation over northern Europe, central Europe, and the Mediterranean relative to the *piControl*. The change in NAO amplitude is found to have positive correlations with the change in DJF mean precipitation over northern and central Europe (Fig. 8a, b) and a negative correlation over the Mediterranean (Fig. 8c). The *lgm* experiment displays a weakened NAO amplitude along with colder mean temperatures, while the other three experiments do not show a clear relationship between the change in NAO amplitude and the temperature change (not shown). Terrestrial proxy data suggest a warmer winter in Europe during the MH (Bartlein et al., 2011) and the LIG (Brewer et al., 2008). However, models do not capture this warming in Europe in both experiments and even present a uniform cooling in the *lig127k*. Mauri et al. (2014) suggested that models do not capture a positive NAO-like pattern due to failing to capture the full extent of high-latitude warming over Northern Europe and underestimate the cold Mediterranean temperatures. This might indicate that the changes in climatological sea level pressure (Fig. 3 right column) are underestimated in the ensemble. Notably, our findings should be interpreted alongside the perspective from Hurrell et al. (2003): although NAO is the dominant mode of atmospheric circulation variability over the North Atlantic, it explains only a fraction of the total variance, and most winters cannot be characterized by the canonical NAO pattern. This implies that while our results highlight NAO's sensitivity to GHG forcing and temperature changes, the actual contribution of NAO variability to European climate may be constrained by its limited explanatory power of total circulation variance.

Earlier studies have noticed a teleconnection existing between ENSO and NAO (Geng et al., 2024; Toniazzo and Scaife, 2006; Hardiman et al., 2019; Zhang et al., 2015; Joshi et al., 2021), though it remains controversial with large uncertainty (López-Parages et al., 2015; Zhang et al., 2019). The ENSO signals reach the North Atlantic region via the stratosphere (Ineson and Scaife, 2009) and tropospheric pathways (Jiménez-Esteve and Domeisen, 2018). Here we investigate whether a weakened/strengthened ENSO could remotely influence the NAO amplitude. The NAO-ENSO relationship responds nonlinearly to changes in ENSO strength (Hardiman et al., 2019). Enhanced ENSO events affect NAO variability by exciting Rossby waves reaching the North Atlantic through strengthened convection anomalies in the Gulf of Mexico and the Caribbean Sea (Ayarzagüena et al., 2018) and in the tropical Indian and Pacific Ocean (Abid et al., 2021; Joshi et al., 2021). Here, we examine the relationship between change in the strength of ENSO, measured as the

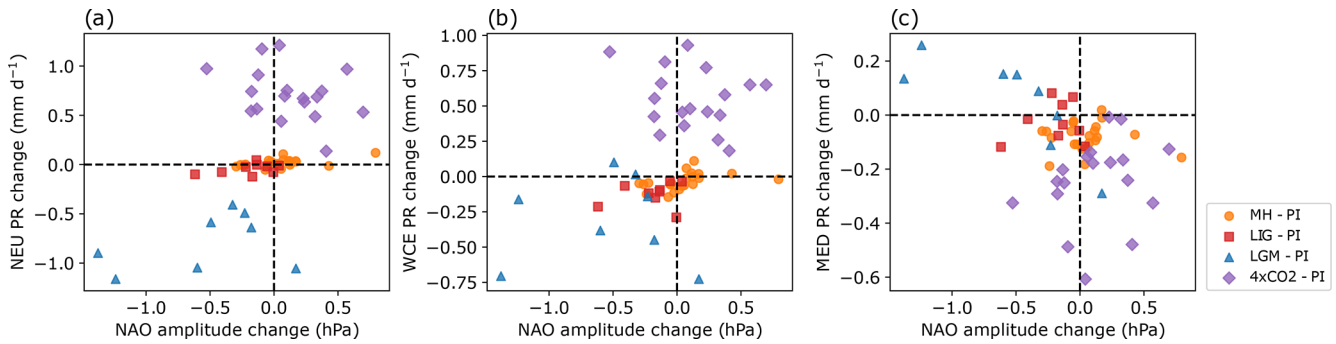


**Figure 8.** Relationships across all experiments and all models between the changes in NAO amplitude and the changes in European mean state of DJF mean precipitation ( $\text{mm d}^{-1}$ ; labelled as PR in panels a to c). Regions follow the definition of IPCC AR6: northern Europe (NEU), west and central Europe (WCE), and Mediterranean (MED). All changes are relative to the *piControl*.

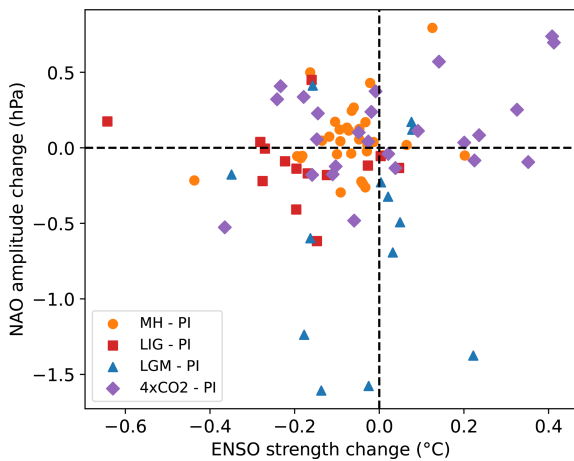


**Figure 9.** Relationship between the change in ENSO strength and NAO amplitude across all models and all experiments relative to the *piControl*. The ENSO strength is measured as the standard deviation of the nino3.4 index of each simulation.

standard deviation of nino3.4 index, and change in NAO amplitude (Fig. 9). Consistent with Brown et al. (2020), ENSO strengths in the two orbital-forced experiments are weakened (more obviously in the *lig127k* experiment), while they are ambiguous in the *lgm* and *abrupt4xCO2* (Fig. 9). In contrast, the NAO amplitude weakens in the *lgm* and its changes are ambiguous in the *abrupt4xCO2*, *midHolocene* and *lig127k* experiments (Fig. 9). There is no clear relationship between the amplitude changes of ENSO and NAO (Fig. 9). It implies that changes in ENSO strength do not remotely influence the NAO amplitude and, therefore, suggest a more nuanced teleconnection than posited by earlier studies.

## 7 Conclusions

We assessed changes in NAO amplitude and teleconnections in a combination of CMIP5 and CMIP6 models. The simulations for past climates include two altered orbital configurations

at the MH (*midHolocene*) and LIG (*lig127k*) and a colder-than-present LGM (*lgm*), and an idealised GHG-forced warming experiment of abrupt quadrupling of  $\text{CO}_2$  (*abrupt4xCO2*). For model evaluation, we compared the *piControl* simulation with the C20 Reanalysis dataset (Compo et al., 2011), as shown in Sect. 3. The *piControl* ensemble reproduces the observed mean state, but with biases. The patterns of the positive phase of the NAO and associated teleconnections are consistent between observation and the *piControl* but with variations across the simulations. We explored changes in NAO spatial patterns and explained variance and amplitude. NAO weakens in response to cooling and strengthens as a result of warming. Some of our results are inconsistent with earlier studies, but the inconsistencies are likely affected by the outputs of a few models. The underlying mechanisms are unclear, but previous studies have highlighted the influence of tropospheric and stratospheric climate changes on NAO behaviour (Rind et al., 2005a, b; Lü et al., 2010). We also discussed changes in NAO teleconnections. The simulated spatial teleconnection patterns associated with the NAO are generally consistent with the theory (see Sect. 1) and are sensitive to the change in NAO amplitude. The *midHolocene* and *lig127k* experiments do not show a clear change in temperature and precipitation associated with the NAO. The weakened NAO in the *lgm* is associated with a cooler and drier northern Europe, while the enhanced NAO in the *abrupt4xCO2* is associated with a warmer and wetter northern Europe as compared to the *piControl*. We did not find the ENSO-NAO teleconnection suggested by other studies. Further work is required to fully understand the underlying mechanisms driving the NAO change and the associated teleconnections.

**Code and data availability.** The processed data for figures are available at [https://github.com/annizhao1994/PMIP\\_NAO](https://github.com/annizhao1994/PMIP_NAO) (last access: 1 March 2026) and <https://doi.org/10.5281/zenodo.15624480> (Zhao, 2026).

**Supplement.** The supplement related to this article is available online at <https://doi.org/10.5194/cp-22-689-2026-supplement>.

**Author contributions.** A.Z. and C.B. performed the bulk of the writing and analysis. V.A-K. put a large effort into the early stage of the analysis. X.S. contributed to the lgm analysis and revised this manuscript. Y.H. revised the manuscript.

**Competing interests.** The contact author has declared that none of the authors has any competing interests.

**Disclaimer.** Publisher's note: Copernicus Publications remains neutral with regard to jurisdictional claims made in the text, published maps, institutional affiliations, or any other geographical representation in this paper. The authors bear the ultimate responsibility for providing appropriate place names. Views expressed in the text are those of the authors and do not necessarily reflect the views of the publisher.

**Acknowledgements.** We acknowledge the modelling groups that donated their simulation output and the Earth System Grid Federation for distributing all that output.

**Financial support.** This research has been supported by the National Natural Science Foundation of China (grant nos. 42488201 and 42505050). X.S. is supported by the Southern Marine Science and Engineering Guangdong Laboratory (Zhuhai) (grant no. SML2023SP204), the Guangdong Basic and Applied Basic Research Foundation (grant no. 2025A1515012165), and the Ocean Negative Carbon Emissions (ONCE) Program.

**Review statement.** This paper was edited by Laurie Menviel and reviewed by Quan Liu and two anonymous referees.

## References

- Abe-Ouchi, A., Saito, F., Kageyama, M., Braconnot, P., Harrison, S. P., Lambeck, K., Otto-Bliesner, B. L., Peltier, W. R., Tarasov, L., Peterschmitt, J.-Y., and Takahashi, K.: Ice-sheet configuration in the CMIP5/PMIP3 Last Glacial Maximum experiments, *Geosci. Model Dev.*, 8, 3621–3637, <https://doi.org/10.5194/gmd-8-3621-2015>, 2015.
- Abid, M. A., Kucharski, F., Molteni, F., Kang, I.-S., Tompkins, A. M., and Almazroui, M.: Separating the Indian and Pacific Ocean Impacts on the Euro-Atlantic Response to ENSO and Its Transition from Early to Late Winter, *J. Climate*, 34, 1531–1548, <https://doi.org/10.1175/JCLI-D-20-0075.1>, 2021.
- Ackerley, D., Reeves, J., Barr, C., Bostock, H., Fitzsimmons, K., Fletcher, M.-S., Gouramanis, C., McGregor, H., Mooney, S., Phipps, S. J., Tibby, J., and Tyler, J.: Evaluation of PMIP2 and PMIP3 simulations of mid-Holocene climate in the Indo-Pacific, Australasian and Southern Ocean regions, *Clim. Past*, 13, 1661–1684, <https://doi.org/10.5194/cp-13-1661-2017>, 2017.
- Argus, D. F., Peltier, W. R., Drummond, R., and Moore, A. W.: The Antarctica component of postglacial rebound model ICE-6G\_C (VM5a) based on GPS positioning, exposure age dating of ice thicknesses, and relative sea level histories, *Geophys. J. Int.*, 198, 537–563, <https://doi.org/10.1093/gji/ggu140>, 2014.
- Ayarzagüena, B., Ineson, S., Dunstone, N. J., Baldwin, M. P., and Scaife, A. A.: Intraseasonal Effects of El Niño–Southern Oscillation on North Atlantic Climate, *J. Climate*, 31, 8861–8873, <https://doi.org/10.1175/JCLI-D-18-0097.1>, 2018.
- Bader, J., Mesquita, M. D. S., Hodges, K. I., Keenlyside, N., Østerhus, S., and Miles, M.: A review on Northern Hemisphere sea-ice, storminess and the North Atlantic Oscillation: Observations and projected changes, *Atmos. Res.*, 101, 809–834, <https://doi.org/10.1016/j.atmosres.2011.04.007>, 2011.
- Balaji, V., Taylor, K. E., Juckes, M., Lawrence, B. N., Durack, P. J., Lautenschlager, M., Blanton, C., Cinquini, L., Denvil, S., Elkington, M., Guglielmo, F., Guilyardi, E., Hassell, D., Kharin, S., Kindermann, S., Nikonov, S., Radhakrishnan, A., Stockhause, M., Weigel, T., and Williams, D.: Requirements for a global data infrastructure in support of CMIP6, *Geosci. Model Dev.*, 11, 3659–3680, <https://doi.org/10.5194/gmd-11-3659-2018>, 2018.
- Bao, Q., Lin, P., Zhou, T., Liu, Y., Yu, Y., Wu, G., He, B., He, J., Li, L., Li, J., Li, C., Liu, H., Qiao, F., Song, Z., Wang, B., Wang, J., Wang, P., Wang, X., Wang, Z., Wu, B., Wu, T., Xu, Y., Yu, H., Zhao, W., Zheng, W., and Zhou, L.: The flexible global ocean-atmosphere-land system model, spectral version 2: FGOALS-s2, *Adv. Atmos. Sci.*, 30, 561–576, <https://doi.org/10.1007/s00376-012-2113-9>, 2013.
- Barlow, N. L. M., McClymont, E. L., Whitehouse, P. L., Stokes, C. R., Jamieson, S. S. R., Woodroffe, S. A., Bentley, M. J., Callard, S. L., Cofaigh, C. Ó., Evans, D. J. A., Horrocks, J. R., Lloyd, J. M., Long, A. J., Margold, M., Roberts, D. H., and Sanchez-Montes, M. L.: Lack of evidence for a substantial sea-level fluctuation within the Last Interglacial, *Nat. Geosci.*, 11, 627–634, <https://doi.org/10.1038/s41561-018-0195-4>, 2018.
- Barnes, E. A. and Polvani, L.: Response of the Midlatitude Jets, and of Their Variability, to Increased Greenhouse Gases in the CMIP5 Models, *J. Climate*, 26, 7117–7135, <https://doi.org/10.1175/JCLI-D-12-00536.1>, 2013.
- Bartlein, P. J. and Shafer, S. L.: Paleo calendar-effect adjustments in time-slice and transient climate-model simulations (PaleoCal-Adjust v1.0): impact and strategies for data analysis, *Geosci. Model Dev.*, 12, 3889–3913, <https://doi.org/10.5194/gmd-12-3889-2019>, 2019.
- Bartlein, P. J., Harrison, S., Brewer, S., Connor, S., Davis, B., Gajewski, K., Guiot, J., Harrison-Prentice, T., Henderson, A., and Peyron, O.: Pollen-based continental climate reconstructions at 6 and 21 ka: a global synthesis, *Clim. Dynam.*, 37, 775–802, <https://doi.org/10.1007/s00382-010-0904-1>, 2011.
- Berger, A.: Long-term variations of caloric insolation resulting from the earth's orbital elements, *Quaternary Res.*, 9, 139–167, 1978.
- Berger, A. and Loutre, M.-F.: Insolation values for the climate of the last 10 million years, *Quaternary Sci. Rev.*, 10, 297–317, 1991.
- Boucher, O., Servonnat, J., Albright, A. L., Aumont, O., Balkanski, Y., Bastrikov, V., Bekki, S., Bonnet, R., Bony, S., Bopp, L., Braconnot, P., Brockmann, P., Cadule, P., Caubel, A., Cheruy, F., Codron, F., Cozic, A., Cugnet, D., D'Andrea, F., Davini, P.,

- Lavergne, C., Denvil, S., Deshayes, J., Devilliers, M., Ducharne, A., Dufresne, J., Dupont, E., Éthé, C., Fairhead, L., Falletti, L., Flavoni, S., Foujols, M., Gardoll, S., Gastineau, G., Ghattas, J., Grandpeix, J., Guenet, B., Guez, Lionel, E., Guilyardi, E., Guimberteau, M., Hauglustaine, D., Hourdin, F., Idelkadi, A., Jous-saume, S., Kageyama, M., Khodri, M., Krinner, G., Lebas, N., Levavasseur, G., Lévy, C., Li, L., Lott, F., Lurton, T., Luys-saert, S., Madec, G., Madeleine, J., Maignan, F., Marchand, M., Marti, O., Mellul, L., Meurdesoif, Y., Mignot, J., Musat, I., Otlé, C., Peylin, P., Planton, Y., Polcher, J., Rio, C., Rochetin, N., Rousset, C., Sepulchre, P., Sima, A., Swingedouw, D., Thiéble-mont, R., Traore, A. K., Vancoppenolle, M., Vial, J., Vialard, J., Viovy, N., and Vuichard, N.: Presentation and Evaluation of the IPSL-CM6A-LR Climate Model, *J. Adv. Model. Earth Sy.*, 12, e2019MS002010, <https://doi.org/10.1029/2019MS002010>, 2020.
- Braconnot, P., Joussaume, S., de Noblet, N., and Ramstein, G.: Mid-Holocene and Last Glacial Maximum African monsoon changes as simulated within the Paleoclimate Modelling Intercomparison Project, *Global Planet. Change*, 26, 51–66, 2000.
- Braconnot, P., Otto-Bliesner, B., Harrison, S., Joussaume, S., Peterchmitt, J.-Y., Abe-Ouchi, A., Crucifix, M., Driesschaert, E., Fichefet, Th., Hewitt, C. D., Kageyama, M., Kitoh, A., Laîné, A., Loutre, M.-F., Marti, O., Merkel, U., Ramstein, G., Valdes, P., Weber, S. L., Yu, Y., and Zhao, Y.: Results of PMIP2 coupled simulations of the Mid-Holocene and Last Glacial Maximum – Part 1: experiments and large-scale features, *Clim. Past*, 3, 261–277, <https://doi.org/10.5194/cp-3-261-2007>, 2007.
- Brewer, S., Guiot, J., Sánchez-Goñi, M. F., and Klotz, S.: The climate in Europe during the Eemian: a multi-method approach using pollen data, *Quaternary Sci. Rev.*, 27, 2303–2315, <https://doi.org/10.1016/j.quascirev.2008.08.029>, 2008.
- Brierley, C. and Wainer, I.: Inter-annual variability in the tropical Atlantic from the Last Glacial Maximum into future climate projections simulated by CMIP5/PMIP3, *Clim. Past*, 14, 1377–1390, <https://doi.org/10.5194/cp-14-1377-2018>, 2018.
- Brierley, C., Thirumalai, K., Grindrod, E., and Barnsley, J.: Indian Ocean variability changes in the Paleoclimate Modelling Intercomparison Project, *Clim. Past*, 19, 681–701, <https://doi.org/10.5194/cp-19-681-2023>, 2023.
- Brierley, C. M., Zhao, A., Harrison, S. P., Braconnot, P., Williams, C. J. R., Thornalley, D. J. R., Shi, X., Peterschmitt, J.-Y., Ohgaito, R., Kaufman, D. S., Kageyama, M., Hargreaves, J. C., Erb, M. P., Emile-Geay, J., D’Agostino, R., Chandan, D., Carré, M., Bartlein, P. J., Zheng, W., Zhang, Z., Zhang, Q., Yang, H., Volodin, E. M., Tomas, R. A., Routson, C., Peltier, W. R., Otto-Bliesner, B., Morozova, P. A., McKay, N. P., Lohmann, G., Legrande, A. N., Guo, C., Cao, J., Brady, E., Annan, J. D., and Abe-Ouchi, A.: Large-scale features and evaluation of the PMIP4-CMIP6 *midHolocene* simulations, *Clim. Past*, 16, 1847–1872, <https://doi.org/10.5194/cp-16-1847-2020>, 2020.
- Brown, J. R., Brierley, C. M., An, S.-I., Guarino, M.-V., Stevenson, S., Williams, C. J. R., Zhang, Q., Zhao, A., Abe-Ouchi, A., Braconnot, P., Brady, E. C., Chandan, D., D’Agostino, R., Guo, C., LeGrande, A. N., Lohmann, G., Morozova, P. A., Ohgaito, R., O’ishi, R., Otto-Bliesner, B. L., Peltier, W. R., Shi, X., Sime, L., Volodin, E. M., Zhang, Z., and Zheng, W.: Comparison of past and future simulations of ENSO in CMIP5/PMIP3 and CMIP6/PMIP4 models, *Clim. Past*, 16, 1777–1805, <https://doi.org/10.5194/cp-16-1777-2020>, 2020.
- Budich, R., Giorgetta, M., Jungclaus, J., Redler, R., and Reick, C.: The MPI-M Millennium Earth System Model: An Assembling Guide for the COSMOS Configuration, Max Planck Institute for Meteorology, [https://pure.mpg.de/rest/items/item\\_2193290/component/file\\_2193291/content](https://pure.mpg.de/rest/items/item_2193290/component/file_2193291/content) (last access: 12 January 2026), 2010.
- Cao, J., Wang, B., Yang, Y.-M., Ma, L., Li, J., Sun, B., Bao, Y., He, J., Zhou, X., and Wu, L.: The NUIST Earth System Model (NESM) version 3: description and preliminary evaluation, *Geosci. Model Dev.*, 11, 2975–2993, <https://doi.org/10.5194/gmd-11-2975-2018>, 2018.
- Clark, P. U. and Mix, A. C.: Ice sheets and sea level of the Last Glacial Maximum, *Quaternary Sci. Rev.*, 21, 1–7, [https://doi.org/10.1016/S0277-3791\(01\)00118-4](https://doi.org/10.1016/S0277-3791(01)00118-4), 2002.
- Clark, P. U., Dyke, A. S., Shakun, J. D., Carlson, A. E., Clark, J., Wohlfarth, B., Mitrovica, J. X., Hostetler, S. W., and McCabe, A. M.: The Last Glacial Maximum, *Science*, 325, 710–714, <https://doi.org/10.1126/science.1172873>, 2009.
- Collins, W. J., Bellouin, N., Doutriaux-Boucher, M., Gedney, N., Halloran, P., Hinton, T., Hughes, J., Jones, C. D., Joshi, M., Liddicoat, S., Martin, G., O’Connor, F., Rae, J., Senior, C., Sitch, S., Totterdell, I., Wiltshire, A., and Woodward, S.: Development and evaluation of an Earth-System model – HadGEM2, *Geosci. Model Dev.*, 4, 1051–1075, <https://doi.org/10.5194/gmd-4-1051-2011>, 2011.
- Compo, G. P., Whitaker, J. S., Sardeshmukh, P. D., Matsui, N., Allan, R. J., Yin, X., Gleason, B. E., Vose, R. S., Rutledge, G., Bessemoulin, P., Brönnimann, S., Brunet, M., Crouthamel, R. I., Grant, A. N., Groisman, P. Y., Jones, P. D., Kruk, M. C., Kruger, A. C., Marshall, G. J., Maugeri, M., Mok, H. Y., Nordli, Ø., Ross, T. F., Trigo, R. M., Wang, X. L., Woodruff, S. D., and Worley, S. J.: The twentieth century reanalysis project, *Q. J. Roy. Meteor. Soc.*, 137, 1–28, <https://doi.org/10.1002/qj.776>, 2011.
- Cook, E. R., Kushnir, Y., Smerdon, J. E., Williams, A. P., Anchukaitis, K. J., and Wahl, E. R.: A Euro-Mediterranean tree-ring reconstruction of the winter NAO index since 910 C.E., *Clim. Dynam.*, 53, 1567–1580, <https://doi.org/10.1007/s00382-019-04696-2>, 2019.
- Cornes, R. C., Jones, P. D., Briffa, K. R., and Osborn, T. J.: Estimates of the North Atlantic Oscillation back to 1692 using a Paris–London westerly index, *Int. J. Climatol.*, 33, 228–248, <https://doi.org/10.1002/joc.3416>, 2013.
- Döscher, R., Acosta, M., Alessandri, A., Anthoni, P., Arsouze, T., Bergman, T., Bernardello, R., Boussetta, S., Caron, L.-P., Carver, G., Castrillo, M., Catalano, F., Cvijanovic, I., Davini, P., Dekker, E., Doblas-Reyes, F. J., Docquier, D., Echevarria, P., Fladrich, U., Fuentes-Franco, R., Gröger, M., v. Hardenberg, J., Hieronymus, J., Karami, M. P., Keskinen, J.-P., Koenigk, T., Makkonen, R., Massonnet, F., Ménégos, M., Miller, P. A., Moreno-Chamarro, E., Nieradzick, L., van Noije, T., Nolan, P., O’Donnell, D., Olinaho, P., van den Oord, G., Ortega, P., Prims, O. T., Ramos, A., Reerink, T., Rousset, C., Ruprich-Robert, Y., Le Sager, P., Schmith, T., Schrödner, R., Serva, F., Sicardi, V., Sloth Madsen, M., Smith, B., Tian, T., Tourigny, E., Uotila, P., Vancoppenolle, M., Wang, S., Wärlind, D., Willén, U., Wyser, K., Yang, S., Yepes-Arbós, X., and Zhang, Q.: The EC-Earth3 Earth system model for the Coupled Model Intercomparison Project 6, *Geosci.*

- Model Dev., 15, 2973–3020, <https://doi.org/10.5194/gmd-15-2973-2022>, 2022.
- Dufresne, J.-L., Foujols, M.-A., Denvil, S., Caubel, A., Marti, O., Aumont, O., Balkanski, Y., Bekki, S., Bellenger, H., Benshila, R., Bony, S., Bopp, L., Braconnot, P., Brockmann, P., Cadule, P., Cheruy, F., Codron, F., Cozic, A., Cugnet, D., de Noblet, N., Duvel, J.-P., Ethé, C., Fairhead, L., Fichefet, T., Flavoni, S., Friedlingstein, P., Grandpeix, J.-Y., Guez, L., Guilyardi, E., Hauglustaine, D., Hourdin, F., Idelkadi, A., Ghattas, J., Jous-saume, S., Kageyama, M., Krinner, G., Labetoulle, S., Lahellec, A., Lefebvre, M.-P., Lefevre, F., Levy, C., Li, Z. X., Lloyd, J., Lott, F., Madec, G., Mancip, M., Marchand, M., Masson, S., Meurdesoif, Y., Mignot, J., Musat, I., Parouty, S., Polcher, J., Rio, C., Schulz, M., Swingedouw, D., Szopa, S., Talandier, C., Terray, P., Viovy, N., and Vuichard, N.: Climate change projections using the IPSL-CM5 Earth System Model: from CMIP3 to CMIP5, *Clim. Dynam.*, 40, 2123–2165, <https://doi.org/10.1007/s00382-012-1636-1>, 2013.
- Eyring, V., Bony, S., Meehl, G. A., Senior, C. A., Stevens, B., Stouffer, R. J., and Taylor, K. E.: Overview of the Coupled Model Intercomparison Project Phase 6 (CMIP6) experimental design and organization, *Geosci. Model Dev.*, 9, 1937–1958, <https://doi.org/10.5194/gmd-9-1937-2016>, 2016.
- Feldstein, S. B. and Franzke, C. L. E.: *Atmospheric Teleconnection Patterns*, Cambridge University Press, Cambridge, 54–104, ISBN 9781107118140, <https://doi.org/10.1017/9781316339251.004>, 2017.
- Flato, G., Marotzke, J., Abiodun, B., Braconnot, P., Chou, S. C., Collins, W., Cox, P., Driouech, F., Emori, S., Eyring, V., Forest, C., Gleckler, P., Guilyardi, E., Jakob, C., Kattsov, V., Reason, C., Rummukainen, M., AchutaRao, K., Anav, A., Andrews, T., Baehr, J., Bindoff, N. L., Bodas-Salcedo, A., Catto, J., Chambers, D., Chang, P., Dai, A., Deser, C., Doblas-Reyes, F., Durack, P. J., Eby, M., de Elia, R., Fichefet, T., Forster, P., Frame, D., Fyfe, J., Gbobaniyi, E., Gillett, N., González-Rouco, J. F., Goodess, C., Griffies, S., Hall, A., Harrison, S., Hense, A., Hunke, E., Ilyina, T., Ivanova, D., Johnson, G., Kageyama, M., Kharin, V., Klein, S. A., Knight, J., Knutti, R., Landerer, F., Lee, T., Li, H., Mahowald, N., Mears, C., Meehl, G., Morice, C., Msadek, R., Myhre, G., Neelin, J. D., Painter, J., Pavlova, T., Perlwitz, J., Peterschmitt, J.-Y., Räisänen, J., Rausser, F., Reid, J., Rodwell, M., Santer, B., Scaife, A. A., Schulz, J., Scinocca, J., Sexton, D., Shindell, D., Shiogama, H., Sillmann, J., Simmons, A., Sperber, K., Stephenson, D., Stevens, B., Stott, P., Sutton, R., Thorne, P. W., van Oldenborgh, G. J., Vecchi, G., Webb, M., Williams, K., Woollings, T., Xie, S.-P., and Zhang, J.: Evaluation of climate models, in: *Climate change 2013: the physical science basis. Contribution of Working Group I to the Fifth Assessment Report of the Intergovernmental Panel on Climate Change*, edited by: Stocker, T., Qin, D., Plattner, G.-K., Tignor, M., Allen, S., Boschung, J., Nauels, A., Xia, Y., Bex, V., and Midgley, P., Cambridge University Press, 741–866, <https://doi.org/10.1017/cbo9781107415324.020>, 2013.
- Funder, S., Goosse, H., Jepsen, H., Kaas, E., Kjær, K. H., Korsgaard, N. J., Larsen, N. K., Linderson, H., Lyså, A., Möller, P., Olsen, J., and Willerslev, E.: A 10,000-Year Record of Arctic Ocean Sea-Ice Variability – View from the Beach, *Science*, 333, 747–750, <https://doi.org/10.1126/science.1202760>, 2011.
- Găinușă-Bogdan, A., Swingedouw, D., Yiou, P., Cattiaux, J., Codron, F., and Michel, S.: AMOC and summer sea ice as key drivers of the spread in mid-holocene winter temperature patterns over Europe in PMIP3 models, *Global Planet. Change*, 184, 103055, <https://doi.org/10.1016/j.gloplacha.2019.103055>, 2020.
- Geng, X., Kug, J.-S., and Kosaka, Y.: Future changes in the winter-time ENSO-NAO teleconnection under greenhouse warming, *npj Clim. Atmos. Sci.*, 7, 81, <https://doi.org/10.1038/s41612-024-00627-z>, 2024.
- Gent, P. R., Danabasoglu, G., Donner, L. J., Holland, M. M., Hunke, E. C., Jayne, S. R., Lawrence, D. M., Neale, R. B., Rasch, P. J., Vertenstein, M., Worley, P. H., Yang, Z.-L., and Zhang, M.: The community climate system model version 4, *J. Climate*, 24, 4973–4991, <https://doi.org/10.1175/2011JCLI4083.1>, 2011.
- Gettelman, A., Hannay, C., Bacmeister, J. T., Neale, R. B., Pendergrass, A. G., Danabasoglu, G., Lamarque, J., Fasullo, J. T., Bailey, D. A., Lawrence, D. M., and Mills, M. J.: High Climate Sensitivity in the Community Earth System Model Version 2 (CESM2), *Geophys. Res. Lett.*, 46, 8329–8337, <https://doi.org/10.1029/2019GL083978>, 2019.
- Giorgetta, M. A., Jungclaus, J., Reick, C. H., Legutke, S., Bader, J., Böttinger, M., Brovkin, V., Crueger, T., Esch, M., Fieg, K., Glushak, K., Gayler, V., Haak, H., Hollweg, H.-D., Ilyina, T., Kinne, S., Kornbluh, L., Matei, D., Mauritsen, T., Mikolajewicz, U., Mueller, W., Notz, D., Pithan, F., Raddatz, T., Rast, S., Redler, R., Roeckner, E., Schmidt, H., Schnur, R., Segsneider, J., Six, K. D., Stockhause, M., Timmreck, C., Wegner, J., Widmann, H., Wieners, K.-H., Claussen, M., Marotzke, J., and Stevens, B.: Climate and carbon cycle changes from 1850 to 2100 in MPI-ESM simulations for the Coupled Model Intercomparison Project phase 5, *J. Adv. Model. Earth Sy.*, 5, 572–597, <https://doi.org/10.1002/jame.20038>, 2013.
- Gladstone, R. M., Ross, I., Valdes, P. J., Abe-Ouchi, A., Braconnot, P., Brewer, S., Kageyama, M., Kitoh, A., Legrande, A., Marti, O., Ohgaito, R., Otto-Bliesner, B., Peltier, W. R., and Vettoretti, G.: Mid-Holocene NAO: A PMIP2 model intercomparison, *Geophys. Res. Lett.*, 32, <https://doi.org/10.1029/2005GL023596>, 2005.
- Govin, A., Braconnot, P., Capron, E., Cortijo, E., Duplessy, J.-C., Jansen, E., Labeyrie, L., Landais, A., Marti, O., Michel, E., Mosquet, E., Risebrobakken, B., Swingedouw, D., and Waelbroeck, C.: Persistent influence of ice sheet melting on high northern latitude climate during the early Last Interglacial, *Clim. Past*, 8, 483–507, <https://doi.org/10.5194/cp-8-483-2012>, 2012.
- Gulev, S. K., Thorne, P., Ahn, J., Dentener, F., Domingues, C., Gerland, S., Gong, D., Kaufman, D., Nnamchi, H., Quaas, J., Rivera, J., Sathyendranath, S., Smith, S., Trewin, B., von Shuckmann, K., and Vose, R.: Changing State of the Climate System, in: *Climate Change 2021: The Physical Science Basis. Contribution of Working Group I to the Sixth Assessment Report of the Intergovernmental Panel on Climate Change*, edited by: Masson-Delmotte, V., Zhai, P., Pirani, A., Connors, S. L., Péan, C., Berger, S., Caud, N., Chen, Y., Goldfarb, L., Gomis, M. I., Huang, M., Leitzell, K., Lonnoy, E., Matthews, J., Maycock, T. K., Waterfield, T., Yelekçi, O., Yu, R., and Zhou, B., Cambridge University Press, Cambridge, United Kingdom and New York, USA, <https://doi.org/10.1017/9781009157896.004>, 2021.
- Guo, C., Bentsen, M., Bethke, I., Ilicak, M., Tjiputra, J., Toni-azzo, T., Schwinger, J., and Otterå, O. H.: Description and eval-

- uation of NorESM1-F: a fast version of the Norwegian Earth System Model (NorESM), *Geosci. Model Dev.*, 12, 343–362, <https://doi.org/10.5194/gmd-12-343-2019>, 2019.
- Hajima, T., Watanabe, M., Yamamoto, A., Tatebe, H., Noguchi, M. A., Abe, M., Ohgaito, R., Ito, A., Yamazaki, D., Okajima, H., Ito, A., Takata, K., Ogochi, K., Watanabe, S., and Kawamiya, M.: Development of the MIROC-ES2L Earth system model and the evaluation of biogeochemical processes and feedbacks, *Geosci. Model Dev.*, 13, 2197–2244, <https://doi.org/10.5194/gmd-13-2197-2020>, 2020.
- Hall, R. J., Mitchell, D. M., Seviour, W. J. M., and Wright, C. J.: Persistent Model Biases in the CMIP6 Representation of Stratospheric Polar Vortex Variability, *J. Geophys. Res.-Atmos.*, 126, e2021JD034759, <https://doi.org/10.1029/2021JD034759>, 2021.
- Hardiman, S. C., Dunstone, N. J., Scaife, A. A., Smith, D. M., Ineson, S., Lim, J., and Fereday, D.: The Impact of Strong El Niño and La Niña Events on the North Atlantic, *Geophys. Res. Lett.*, 46, 2874–2883, <https://doi.org/10.1029/2018GL081776>, 2019.
- Harrison, S. P., Bartlein, P., Izumi, K., Li, G., Annan, J., Hargreaves, J., Braconnot, P., and Kageyama, M.: Evaluation of CMIP5 palaeo-simulations to improve climate projections, *Nat. Clim. Change*, 5, 735–743, <https://doi.org/10.1038/nclimate2649>, 2015.
- Harvey, B. J., Shaffrey, L. C., and Woollings, T. J.: Equator-to-pole temperature differences and the extra-tropical storm track responses of the CMIP5 climate models, *Clim. Dynam.*, 43, 1171–1182, <https://doi.org/10.1007/s00382-013-1883-9>, 2014.
- Harvey, B. J., Shaffrey, L. C., and Woollings, T. J.: Deconstructing the climate change response of the Northern Hemisphere wintertime storm tracks, *Clim. Dynam.*, 45, 2847–2860, <https://doi.org/10.1007/s00382-015-2510-8>, 2015.
- Hazeleger, W., Wang, X., Severijns, C., Stefanescu, S., Bintanja, R., Sterl, A., Wyser, K., Semmler, T., Yang, S., Van den Hurk, B., van Noije, T., van der Linden, E., and van der Wiel, K.: EC-Earth V2. 2: description and validation of a new seamless earth system prediction model, *Clim. Dynam.*, 39, 2611–2629, <https://doi.org/10.1007/s00382-011-1228-5>, 2012.
- He, B., Yu, Y., Bao, Q., Lin, P., Liu, H., Li, J., Wang, L., Liu, Y., Wu, G., Chen, K., Guo, Y., Zhao, S., Zhang, X., Song, M., and Xie, J.: CAS FGOALS-f3-L Model dataset descriptions for CMIP6 DECK experiments, *Atmos. Ocean. Sc. Lett.*, 13, 582–588, <https://doi.org/10.1080/16742834.2020.1778419>, 2020.
- Henderson, G. R., Peings, Y., Furtado, J. C., and Kushner, P. J.: Snow–atmosphere coupling in the Northern Hemisphere, *Nat. Clim. Change*, 8, 954–963, <https://doi.org/10.1038/s41558-018-0295-6>, 2018.
- Hernández, A., Martín-Puertas, C., Moffa-Sánchez, P., Moreno-Chamarro, E., Ortega, P., Blockley, S., Cobb, K. M., Comas-Bru, L., Giralt, S., Goosse, H., Luterbacher, J., Martrat, B., Muscheler, R., Parnell, A., Pla-Rabes, S., Sjolte, J., Scaife, A. A., Swingedouw, D., Wise, E., and Xu, G.: Modes of climate variability: Synthesis and review of proxy-based reconstructions through the Holocene, *Earth-Sci. Rev.*, 209, 103286, <https://doi.org/10.1016/j.earscirev.2020.103286>, 2020.
- Hurrell, J. W., Kushnir, Y., Ottersen, G., and Visbeck, M.: An Overview of the North Atlantic Oscillation, *American Geophysical Union (AGU)*, 1–35, ISBN 9781118669037, <https://doi.org/10.1029/134GM01>, 2003.
- Hurrell, J. W., Hoerling, M. P., Phillips, A. S., and Xu, T.: Twentieth century north atlantic climate change. Part I: assessing determinism, *Clim. Dynam.*, 23, 371–389, <https://doi.org/10.1007/s00382-004-0432-y>, 2004.
- Ineson, S. and Scaife, A. A.: The role of the stratosphere in the European climate response to El Niño, *Nat. Geosci.*, 2, 32–36, <https://doi.org/10.1038/ngeo381>, 2009.
- IPCC: Annex II: Models, edited by: Gutiérrez, J. M. and Tréguier, A.-M., in: *Climate Change 2021: The Physical Science Basis. Contribution of Working Group I to the Sixth Assessment Report of the Intergovernmental Panel on Climate Change*, edited by: Masson-Delmotte, V., Zhai, P., Pirani, A., Connors, S. L., Péan, C., Berger, S., Caud, N., Chen, Y., Goldfarb, L., Gomis, M. I., Huang, M., Leitzell, K., Lonnoy, E., Matthews, J., Maycock, T. K., Waterfield, T., Yelekçi, O., Yu, R., and Zhou, B., Cambridge University Press, Cambridge, United Kingdom and New York, USA, <https://doi.org/10.1017/9781009157896.016>, 2021a.
- IPCC: Annex IV: Modes of Variability, edited by: Cassou, C., Cherchi, A., and Kosaka, Y., in: *Climate Change 2021: The Physical Science Basis. Contribution of Working Group I to the Sixth Assessment Report of the Intergovernmental Panel on Climate Change*, edited by: Masson-Delmotte, V., Zhai, P., Pirani, A., Connors, S. L., Péan, C., Berger, S., Caud, N., Chen, Y., Goldfarb, L., Gomis, M. I., Huang, M., Leitzell, K., Lonnoy, E., Matthews, J., Maycock, T. K., Waterfield, T., Yelekçi, O., Yu, R., and Zhou, B., Cambridge University Press, Cambridge, United Kingdom and New York, USA, <https://doi.org/10.1017/9781009157896.018>, 2021b.
- Ivanovic, R. F., Gregoire, L. J., Kageyama, M., Roche, D. M., Valdes, P. J., Burke, A., Drummond, R., Peltier, W. R., and Tarasov, L.: Transient climate simulations of the deglaciation 21–9 thousand years before present (version 1) – PMIP4 Core experiment design and boundary conditions, *Geosci. Model Dev.*, 9, 2563–2587, <https://doi.org/10.5194/gmd-9-2563-2016>, 2016.
- Jiménez-Esteve, B. and Domeisen, D. I. V.: The Tropospheric Pathway of the ENSO–North Atlantic Teleconnection, *J. Climate*, 31, 4563–4584, <https://doi.org/10.1175/JCLI-D-17-0716.1>, 2018.
- Jones, P. D., Jonsson, T., and Wheeler, D.: Extension to the North Atlantic oscillation using early instrumental pressure observations from Gibraltar and south-west Iceland, *Int. J. Climatol.*, 17, 1433–1450, [https://doi.org/10.1002/\(SICI\)1097-0088\(19971115\)17:13<1433::AID-JOC203>3.0.CO;2-P](https://doi.org/10.1002/(SICI)1097-0088(19971115)17:13<1433::AID-JOC203>3.0.CO;2-P), 1997.
- Jonkers, L., Laepple, T., Rillo, M. C., Shi, X., Dolman, A. M., Lohmann, G., Paul, A., Mix, A., and Kucera, M.: Strong temperature gradients in the ice age North Atlantic Ocean revealed by plankton biogeography, *Nat. Geosci.*, 16, 1114–1119, <https://doi.org/10.1038/s41561-023-01328-7>, 2023.
- Joshi, M. K., Abid, M. A., and Kucharski, F.: The Role of an Indian Ocean Heating Dipole in the ENSO Teleconnection to the North Atlantic European Region in Early Winter during the Twentieth Century in Reanalysis and CMIP5 Simulations, *J. Climate*, 34, 1047–1060, <https://doi.org/10.1175/JCLI-D-20-0269.1>, 2021.
- Joussaume, S. and Taylor, K. E.: Status of the Paleoclimate Modelling Intercomparison Project (PMIP), *Proceedings of the first international AMIP scientific conference*, 425–430, WCRP-92, WMO/TD-732, 1995.
- Juckles, M., Taylor, K. E., Durack, P. J., Lawrence, B., Mizielinski, M. S., Pamment, A., Peterschmitt, J.-Y., Rixen, M., and Sénési, S.: The CMIP6 Data Request (DREQ, version 01.00.31), *Geosci.*

- Model Dev., 13, 201–224, <https://doi.org/10.5194/gmd-13-201-2020>, 2020.
- Justino, F. and Peltier, W. R.: The glacial North Atlantic Oscillation, *Geophys. Res. Lett.*, 32, <https://doi.org/10.1029/2005GL023822>, 2005.
- Kageyama, M., Braconnot, P., Harrison, S. P., Haywood, A. M., Jungclaus, J. H., Otto-Bliesner, B. L., Peterschmitt, J.-Y., Abe-Ouchi, A., Albani, S., Bartlein, P. J., Brierley, C., Crucifix, M., Dolan, A., Fernandez-Donado, L., Fischer, H., Hopcroft, P. O., Ivanovic, R. F., Lambert, F., Lunt, D. J., Mahowald, N. M., Peltier, W. R., Phipps, S. J., Roche, D. M., Schmidt, G. A., Tarasov, L., Valdes, P. J., Zhang, Q., and Zhou, T.: The PMIP4 contribution to CMIP6 – Part 1: Overview and overarching analysis plan, *Geosci. Model Dev.*, 11, 1033–1057, <https://doi.org/10.5194/gmd-11-1033-2018>, 2018.
- Kageyama, M., Harrison, S. P., Kapsch, M.-L., Lofverstrom, M., Lora, J. M., Mikolajewicz, U., Sherriff-Tadano, S., Vadsaria, T., Abe-Ouchi, A., Bouttes, N., Chandan, D., Gregoire, L. J., Ivanovic, R. F., Izumi, K., LeGrande, A. N., Lhardy, F., Lohmann, G., Morozova, P. A., Ohgaito, R., Paul, A., Peltier, W. R., Poulsen, C. J., Quiquet, A., Roche, D. M., Shi, X., Tierney, J. E., Valdes, P. J., Volodin, E., and Zhu, J.: The PMIP4 Last Glacial Maximum experiments: preliminary results and comparison with the PMIP3 simulations, *Clim. Past*, 17, 1065–1089, <https://doi.org/10.5194/cp-17-1065-2021>, 2021.
- Kelley, M., Schmidt, G. A., Nazarenko, L., Bauer, S. E., Ruedy, R., Russell, G. L., Ackerman, A. S., Aleinov, I., Bauer, M., Bleck, R., Canuto, V., Cesana, G., Cheng, Y., Clune, T. L., Cook, B. I., Cruz, C. A., Del Genio, A. D., Elsaesser, G. S., Faluvegi, G., Kiang, N. Y., Kim, D., Lacis, A. A., Leboissetier, A., LeGrande, A. N., Lo, K. K., Marshall, J., Matthews, E. E., McDermid, S., Mezuman, K., Miller, R. L., Murray, L. T., Oinas, V., Orbe, C., Pérez García-Pando, C., Perlwitz, J. P., Puma, M. J., Rind, D., Romanou, A., Shindell, D. T., Sun, S., Tausnev, N., Tsigaridis, K., Tselioudis, G., Weng, E., Wu, J., and Yao, M.-S.: GISS-E2.1: Configurations and climatology, *J. Adv. Model. Earth Syst.*, 12, e2019MS002025, <https://doi.org/10.1029/2019MS002025>, 2020.
- Khosravi, N., Wang, Q., Koldunov, N., Hinrichs, C., Semmler, T., Danilov, S., and Jung, T.: The Arctic Ocean in CMIP6 Models: Biases and Projected Changes in Temperature and Salinity, *Earths Future*, 10, e2021EF002282, <https://doi.org/10.1029/2021EF002282>, 2022.
- Kimoto, M., Jin, F.-F., Watanabe, M., and Yasutomi, N.: Zonal – eddy coupling and a neutral mode theory for the Arctic Oscillation, *Geophys. Res. Lett.*, 28, 737–740, <https://doi.org/10.1029/2000GL012377>, 2001.
- Lee, J. Y., Marotzke, J., Bala, G., Cao, L., Corti, S., Dunne, J., Engelbrecht, F., Fischer, E., Fyfe, J., Jones, C., Maycock, A., Mutemi, J., Ndiaye, O., Panickal, S., and Zhou, T.: Future Global Climate: Scenario-Based Projections and Near-Term Information, in: *Climate Change 2021: The Physical Science Basis. Contribution of Working Group I to the Sixth Assessment Report of the Intergovernmental Panel on Climate Change*, edited by: Masson-Delmotte, V., Zhai, P., Pirani, A., Connors, S. L., Péan, C., Berger, S., Caud, N., Chen, Y., Goldfarb, L., Gomis, M. I., Huang, M., Leitzell, K., Lonnoy, E., Matthews, J., Maycock, T. K., Waterfield, T., Yelekçi, O., Yu, R., and Zhou, B., Cambridge University Press, <https://doi.org/10.1017/9781009157896.006>, 2021.
- Li, L., Lin, P., Yu, Y., Wang, B., Zhou, T., Liu, L., Liu, J., Bao, Q., Xu, S., Huang, W., Xia, K., Pu, Y., Dong, L., Shen, S., Liu, Y., Hu, N., Liu, M., Sun, W., Shi, X., Zheng, W., Wu, B., Song, M., Liu, H., Zhang, X., Wu, G., Xue, W., Huang, X., Yang, G., Song, Z., and Qiao, F.: The flexible global ocean-atmosphere-land system model, Grid-point Version 2: FGOALS-g2, *Adv. Atmos. Sci.*, 30, 543–560, <https://doi.org/10.1007/s00376-012-2140-6>, 2013.
- Li, L., Yu, Y., Tang, Y., Lin, P., Xie, J., Song, M., Dong, L., Zhou, T., Liu, L., Wang, L., Pu, Y., Chen, X., Chen, L., Xie, Z., Liu, H., Zhang, L., Huang, X., Feng, T., Zheng, W., Xia, K., Liu, H., Liu, J., Wang, Y., Wang, L., Jia, B., Xie, F., Wang, B., Zhao, S., Yu, Z., Zhao, B., and Wei, J.: The Flexible Global Ocean-Atmosphere-Land System Model Grid-Point Version 3 (FGOALS-g3): Description and Evaluation, *J. Adv. Model. Earth Sy.*, 12, e2019MS002012, <https://doi.org/10.1029/2019MS002012>, 2020.
- López-Parages, J., Rodríguez-Fonseca, B., and Terray, L.: A mechanism for the multidecadal modulation of ENSO teleconnection with Europe, *Clim. Dynam.*, 45, 867–880, <https://doi.org/10.1007/s00382-014-2319-x>, 2015.
- Lorenz, D. J. and DeWeaver, E. T.: Tropopause height and zonal wind response to global warming in the IPCC scenario integrations, *J. Geophys. Res.-Atmos.*, 112, <https://doi.org/10.1029/2006JD008087>, 2007.
- Lorenz, D. J. and Hartmann, D. L.: Eddy–Zonal Flow Feedback in the Northern Hemisphere Winter, *J. Climate*, 16, 1212–1227, [https://doi.org/10.1175/1520-0442\(2003\)16<1212:EFFFITN>2.0.CO;2](https://doi.org/10.1175/1520-0442(2003)16<1212:EFFFITN>2.0.CO;2), 2003.
- Lü, J.-M., Kim, S.-J., Abe-Ouchi, A., Yu, Y., and Ohgaito, R.: Arctic Oscillation during the Mid-Holocene and Last Glacial Maximum from PMIP2 Coupled Model Simulations, *J. Climate*, 23, 3792–3813, <https://doi.org/10.1175/2010JCLI3331.1>, 2010.
- Madan, G., Gjermundsen, A., Iversen, S. C., and LaCasce, J. H.: The weakening AMOC under extreme climate change, *Clim. Dynam.*, 62, 1291–1309, <https://doi.org/10.1007/s00382-023-06957-7>, 2024.
- Marino, G., Rohling, E. J., Rodríguez-Sanz, L., Grant, K. M., Heslop, D., Roberts, A. P., Stanford, J. D., and Yu, J.: Bipolar seesaw control on last interglacial sea level, *Nature*, 522, 197–201, <https://doi.org/10.1038/nature14499>, 2015.
- Marshall, J., Johnson, H., and Goodman, J.: A Study of the Interaction of the North Atlantic Oscillation with Ocean Circulation, *J. Climate*, 14, 1399–1421, [https://doi.org/10.1175/1520-0442\(2001\)014<1399:ASOTIO>2.0.CO;2](https://doi.org/10.1175/1520-0442(2001)014<1399:ASOTIO>2.0.CO;2), 2001.
- Mauri, A., Davis, B. A. S., Collins, P. M., and Kaplan, J. O.: The influence of atmospheric circulation on the mid-Holocene climate of Europe: a data–model comparison, *Clim. Past*, 10, 1925–1938, <https://doi.org/10.5194/cp-10-1925-2014>, 2014.
- Mauritsen, T., Bader, J., Becker, T., Behrens, J., Bittner, M., Brokopf, R., Brovkin, V., Claussen, M., Crueger, T., Esch, M., Fast, I., Fiedler, S., Fläschner, D., Gayler, V., Giorgetta, M., Goll, D. S., Haak, H., Hagemann, S., Hedemann, C., Hohenegger, C., Ilyina, T., Jahns, T., Jimenez-de-la Cuesta, D., Jungclaus, J., Kleinen, T., Kloster, S., Kracher, D., Kinne, S., Kleberg, D., Lasslop, G., Kornbluh, L., Marotzke, J., Matei, D., Meraner, K., Mikolajewicz, U., Modali, K., Möbis, B., Müller, W. A., Nabel,

- J. E. M. S., Nam, C. C. W., Notz, D., Nyawira, S.-S., Paulsen, H., Peters, K., Pincus, R., Pohlmann, H., Pongratz, J., Popp, M., Raddatz, T. J., Rast, S., Redler, R., Reick, C. H., Rohrschneider, T., Schemann, V., Schmidt, H., Schnur, R., Schulzweida, U., Six, K. D., Stein, L., Stemmler, I., Stevens, B., von Storch, J.-S., Tian, F., Voigt, A., Vrese, P., Wieners, K.-H., Wilkenskjaeld, S., Winkler, A., and Roeckner, E.: Developments in the MPI-M Earth System Model version 1.2 (MPI-ESM1.2) and Its Response to Increasing CO<sub>2</sub>, *J. Adv. Model. Earth Sy.*, 11, 998–1038, <https://doi.org/10.1029/2018MS001400>, 2019.
- McKenna, C. M. and Maycock, A. C.: Sources of Uncertainty in Multimodel Large Ensemble Projections of the Winter North Atlantic Oscillation, *Geophys. Res. Lett.*, 48, e2021GL093258, <https://doi.org/10.1029/2021GL093258>, 2021.
- Michel, S., Swingedouw, D., Chavent, M., Ortega, P., Mignot, J., and Khodri, M.: Reconstructing climatic modes of variability from proxy records using ClimIndRec version 1.0, *Geosci. Model Dev.*, 13, 841–858, <https://doi.org/10.5194/gmd-13-841-2020>, 2020.
- Miller, R. L., Schmidt, G. A., and Shindell, D. T.: Forced annular variations in the 20th century Intergovernmental Panel on Climate Change Fourth Assessment Report models, *J. Geophys. Res.-Atmos.*, 111, <https://doi.org/10.1029/2005JD006323>, 2006.
- Mosedale, T. J., Stephenson, D. B., Collins, M., and Mills, T. C.: Granger Causality of Coupled Climate Processes: Ocean Feedback on the North Atlantic Oscillation, *J. Climate*, 19, 1182–1194, <https://doi.org/10.1175/JCLI3653.1>, 2006.
- Omrani, N.-E., Keenlyside, N., Matthes, K., Boljka, L., Zanchettin, D., Jungclaus, J. H., and Lubis, S. W.: Coupled stratosphere-troposphere-Atlantic multidecadal oscillation and its importance for near-future climate projection, *npj Clim. Atmos. Sci.*, 5, 59, <https://doi.org/10.1038/s41612-022-00275-1>, 2022.
- Osborn, T. J.: Simulating the winter North Atlantic Oscillation: the roles of internal variability and greenhouse gas forcing, *Clim. Dynam.*, 22, 605–623, <https://doi.org/10.1007/s00382-004-0405-1>, 2004.
- Otto-Bliesner, B. L., Brady, E. C., Clauzet, G., Tomas, R., Levis, S., and Kothavala, Z.: Last Glacial Maximum and Holocene Climate in CCSM3, *J. Climate*, 19, 2526–2544, <https://doi.org/10.1175/JCLI3748.1>, 2006.
- Otto-Bliesner, B. L., Braconnot, P., Harrison, S. P., Lunt, D. J., Abe-Ouchi, A., Albani, S., Bartlein, P. J., Capron, E., Carlson, A. E., Dutton, A., Fischer, H., Goelzer, H., Govin, A., Haywood, A., Joos, F., LeGrande, A. N., Lipscomb, W. H., Lohmann, G., Mahowald, N., Nehrbaas-Ahles, C., Pausata, F. S. R., Peterschmitt, J.-Y., Phipps, S. J., Renssen, H., and Zhang, Q.: The PMIP4 contribution to CMIP6 – Part 2: Two interglacials, scientific objective and experimental design for Holocene and Last Interglacial simulations, *Geosci. Model Dev.*, 10, 3979–4003, <https://doi.org/10.5194/gmd-10-3979-2017>, 2017.
- Otto-Bliesner, B. L., Brady, E. C., Tomas, R. A., Albani, S., Bartlein, P. J., Mahowald, N. M., Shafer, S. L., Kluzek, E., Lawrence, P. J., Leguy, G., Rothstein, M., and Sommers, A.: A Comparison of the CMIP6 midHolocene and lig127k Simulations in CESM2, *Paleoceanography and Paleoclimatology*, 35, e2020PA003957, <https://doi.org/10.1029/2020PA003957>, 2020.
- Otto-Bliesner, B. L., Brady, E. C., Zhao, A., Brierley, C. M., Axford, Y., Capron, E., Govin, A., Hoffman, J. S., Isaacs, E., Kageyama, M., Scussolini, P., Tzedakis, P. C., Williams, C. J. R., Wolff, E., Abe-Ouchi, A., Braconnot, P., Ramos Buarque, S., Cao, J., de Vernal, A., Guarino, M. V., Guo, C., LeGrande, A. N., Lohmann, G., Meissner, K. J., Menviel, L., Morozova, P. A., Nisancioglu, K. H., O’ishi, R., Salas y Méliá, D., Shi, X., Sicard, M., Sime, L., Stepanek, C., Tomas, R., Volodin, E., Yeung, N. K. H., Zhang, Q., Zhang, Z., and Zheng, W.: Large-scale features of Last Interglacial climate: results from evaluating the *lig127k* simulations for the Coupled Model Intercomparison Project (CMIP6)–Paleoclimate Modeling Intercomparison Project (PMIP4), *Clim. Past*, 17, 63–94, <https://doi.org/10.5194/cp-17-63-2021>, 2021.
- Oudar, T., Sanchez-Gomez, E., Chauvin, F., Cattiaux, J., Terray, L., and Cassou, C.: Respective roles of direct GHG radiative forcing and induced Arctic sea ice loss on the Northern Hemisphere atmospheric circulation, *Clim. Dynam.*, 49, 3693–3713, <https://doi.org/10.1007/s00382-017-3541-0>, 2017.
- Park, W., Keenlyside, N., Latif, M., Ströh, A., Redler, R., Roeckner, E., and Madec, G.: Tropical Pacific Climate and Its Response to Global Warming in the Kiel Climate Model, *J. Climate*, 22, 71–92, <https://doi.org/10.1175/2008JCLI2261.1>, 2009.
- Pedersen, R. A., Cvijanovic, I., Langen, P. L., and Vinther, B. M.: The Impact of Regional Arctic Sea Ice Loss on Atmospheric Circulation and the NAO, *J. Climate*, 29, 889–902, <https://doi.org/10.1175/JCLI-D-15-0315.1>, 2016.
- Peings, Y., Cattiaux, J., Vavrus, S., and Magnusdottir, G.: Late Twenty-First-Century Changes in the Midlatitude Atmospheric Circulation in the CESM Large Ensemble, *J. Climate*, 30, 5943–5960, <https://doi.org/10.1175/JCLI-D-16-0340.1>, 2017.
- Peltier, W. R. and Vettoretti, G.: Dansgaard-Oeschger oscillations predicted in a comprehensive model of glacial climate: A “kicked” salt oscillator in the Atlantic, *Geophys. Res. Lett.*, 41, 7306–7313, <https://doi.org/10.1002/2014GL061413>, 2014.
- Peltier, W. R., Argus, D. F., and Drummond, R.: Space geodesy constrains ice age terminal deglaciation: The global ICE-6G\_C (VM5a) model, *J. Geophys. Res.-Sol. Ea.*, 120, 450–487, <https://doi.org/10.1002/2014JB011176>, 2015.
- Phipps, S. J., Rotstayn, L. D., Gordon, H. B., Roberts, J. L., Hirst, A. C., and Budd, W. F.: The CSIRO Mk3L climate system model version 1.0 – Part 2: Response to external forcings, *Geosci. Model Dev.*, 5, 649–682, <https://doi.org/10.5194/gmd-5-649-2012>, 2012.
- Rimbu, N., Lohmann, G., Kim, J. H., Arz, H. W., and Schneider, R.: Arctic/North Atlantic Oscillation signature in Holocene sea surface temperature trends as obtained from alkenone data, *Geophys. Res. Lett.*, 30, <https://doi.org/10.1029/2002GL016570>, 2003.
- Rind, D., Perlwitz, J., and Lonergan, P.: AO/NAO response to climate change: 1. Respective influences of stratospheric and tropospheric climate changes, *J. Geophys. Res.-Atmos.*, 110, <https://doi.org/10.1029/2004JD005103>, 2005a.
- Rind, D., Perlwitz, J., Lonergan, P., and Lerner, J.: AO/NAO response to climate change: 2. Relative importance of low- and high-latitude temperature changes, *J. Geophys. Res.-Atmos.*, 110, <https://doi.org/10.1029/2004JD005686>, 2005b.
- Rotstayn, L. D., Collier, M. A., Mitchell, R. M., Qin, Y., Campbell, S. K., and Dravitzki, S. M.: Simulated enhancement of ENSO-related rainfall variability due to Australian dust, *Atmos. Chem. Phys.*, 11, 6575–6592, <https://doi.org/10.5194/acp-11-6575-2011>, 2011.

- Schmidt, G. A., Kelley, M., Nazarenko, L., Ruedy, R., Russell, G. L., Aleinov, I., Bauer, M., Bauer, S. E., Bhat, M. K., Bleck, R., Canuto, V., Chen, Y.-H., Cheng, Y., Clune, T. L., Del Genio, A., de Fainchtein, R., Faluvegi, G., Hansen, J. E., Healy, R. J., Kiang, N. Y., Koch, D., Lacis, A. A., LeGrande, A. N., Lerner, J., Lo, K. K., Matthews, E. E., Menon, S., Miller, R. L., Oinas, V., Oloso, A. O., Perlwitz, J. P., Puma, M. J., Putman, W. M., Rind, D., Romanou, A., Sato, M., Shindell, D. T., Sun, S., Syed, R. A., Tausnev, N., Tsigaridis, K., Unger, N., Voulgarakis, A., Yao, M.-S., and Zhang, J.: Configuration and assessment of the GISS ModelE2 contributions to the CMIP5 archive, *J. Adv. Model. Earth Sy.*, 6, 141–184, <https://doi.org/10.1002/2013MS000265>, 2014.
- Screen, J. A., Bracegirdle, T. J., and Simmonds, I.: Polar Climate Change as Manifest in Atmospheric Circulation, *Current Climate Change Reports*, 4, 383–395, <https://doi.org/10.1007/s40641-018-0111-4>, 2018.
- Seland, Ø., Bentsen, M., Olivié, D., Toniazzo, T., Gjermundsen, A., Graff, L. S., Debernard, J. B., Gupta, A. K., He, Y.-C., Kirkevåg, A., Schwinger, J., Tjiputra, J., Aas, K. S., Bethke, I., Fan, Y., Griesfeller, J., Grini, A., Guo, C., Ilicak, M., Karset, I. H. H., Landgren, O., Liakka, J., Moseid, K. O., Nummelin, A., Spensberger, C., Tang, H., Zhang, Z., Heinze, C., Iversen, T., and Schulz, M.: Overview of the Norwegian Earth System Model (NorESM2) and key climate response of CMIP6 DECK, historical, and scenario simulations, *Geosci. Model Dev.*, 13, 6165–6200, <https://doi.org/10.5194/gmd-13-6165-2020>, 2020.
- Serreze, M. C. and Barry, R. G.: Processes and impacts of Arctic amplification: A research synthesis, *Global Planet. Change*, 77, 85–96, <https://doi.org/10.1016/j.gloplacha.2011.03.004>, 2011.
- Shi, X., Werner, M., Yang, H., D'Agostino, R., Liu, J., Yang, C., and Lohmann, G.: Unraveling the complexities of the Last Glacial Maximum climate: the role of individual boundary conditions and forcings, *Clim. Past*, 19, 2157–2175, <https://doi.org/10.5194/cp-19-2157-2023>, 2023.
- Sidorenko, D., Rackow, T., Jung, T., Semmler, T., Barbi, D., Danilov, S., Dethloff, K., Dorn, W., Fieg, K., Goessling, H. F., Handorf, D., Harig, S., Hiller, W., Juricke, S., Losch, M., Schröter, J., Sein, D. V., and Wang, Q.: Towards multi-resolution global climate modeling with ECHAM6–FESOM. Part I: model formulation and mean climate, *Clim. Dynam.*, 44, 757–780, <https://doi.org/10.1007/s00382-014-2290-6>, 2015.
- Smith, D. M., Dunstone, N. J., Scaife, A. A., Fiedler, E. K., Copsey, D., and Hardiman, S. C.: Atmospheric Response to Arctic and Antarctic Sea Ice: The Importance of Ocean–Atmosphere Coupling and the Background State, *J. Climate*, 30, 4547–4565, <https://doi.org/10.1175/JCLI-D-16-0564.1>, 2017.
- Spencer, M. and Essery, R.: Scottish snow cover dependence on the North Atlantic Oscillation index, *Hydrol. Res.*, 47, 619–629, <https://doi.org/10.2166/nh.2016.085>, 2016.
- Stephenson, D. B., Pavan, V., Collins, M., Junge, M. M., Quadrelli, R., and Groups, P. C. M.: North Atlantic Oscillation response to transient greenhouse gas forcing and the impact on European winter climate: a CMIP2 multi-model assessment, *Clim. Dynam.*, 27, 401–420, <https://doi.org/10.1007/s00382-006-0140-x>, 2006.
- Sueyoshi, T., Ohgaito, R., Yamamoto, A., Chikamoto, M. O., Hajima, T., Okajima, H., Yoshimori, M., Abe, M., O'ishi, R., Saito, F., Watanabe, S., Kawamiya, M., and Abe-Ouchi, A.: Set-up of the PMIP3 paleoclimate experiments conducted using an Earth system model, *MIROC-ESM*, *Geosci. Model Dev.*, 6, 819–836, <https://doi.org/10.5194/gmd-6-819-2013>, 2013.
- Taylor, K. E., Stouffer, R. J., and Meehl, G. A.: An Overview of CMIP5 and the Experiment Design, *B. Am. Meteorol. Soc.*, 93, 485–498, <https://doi.org/10.1175/BAMS-D-11-00094.1>, 2012.
- Toniazzo, T. and Scaife, A. A.: The influence of ENSO on winter North Atlantic climate, *Geophys. Res. Lett.*, 33, <https://doi.org/10.1029/2006GL027881>, 2006.
- Vallis, G. K., Zurita-Gotor, P., Cairns, C., and Kidston, J.: Response of the large-scale structure of the atmosphere to global warming, *Q. J. Roy. Meteor. Soc.*, 141, 1479–1501, <https://doi.org/10.1002/qj.2456>, 2015.
- Vinther, B. M., Andersen, K. K., Hansen, A. W., Schmith, T., and Jones, P. D.: Improving the Gibraltar/Reykjavik NAO index, *Geophys. Res. Lett.*, 30, <https://doi.org/10.1029/2003GL018220>, 2003.
- Voltaire, A., Sanchez-Gomez, E., y Méliá, D. S., Decharme, B., Cassou, C., Sénési, S., Valcke, S., Beau, I., Alias, A., Chevallier, M., Déqué, M., Deshayes, J., Douville, H., Fernandez, E., Madec, G., Maisonnave, E., Moine, M.-P., Planton, S., Saint-Martin, D., Szopa, S., Tyteca, S., Alkama, R., Belamari, S., Braun, A., Coquart, L., and Chauvin, F.: The CNRM-CM5.1 global climate model: description and basic evaluation, *Clim. Dynam.*, 40, 2091–2121, <https://doi.org/10.1007/s00382-011-1259-y>, 2013.
- Voltaire, A., Saint-Martin, D., Sénési, S., Decharme, B., Alias, A., Chevallier, M., Colin, J., Guérémy, J., Michou, M., Moine, M., Nabat, P., Roehrig, R., y Méliá, D. S., Sférian, R., Valcke, S., Beau, I., Belamari, S., Berthet, S., Cassou, C., Cattiaux, J., Deshayes, J., Douville, H., Ethé, C., Franchistéguy, L., Geoffroy, O., Lévy, C., Madec, G., Meurdesoif, Y., Msadek, R., Ribes, A., Sanchez-Gomez, E., Terray, L., and Waldman, R.: Evaluation of CMIP6 DECK Experiments With CNRM-CM6-1, *J. Adv. Model. Earth Sy.*, 11, 2177–2213, <https://doi.org/10.1029/2019MS001683>, 2019.
- Volodin, E. M., Mortikov, E. V., Kostykin, S. V., Galin, V. Y., Lykossov, V. N., Gritsun, A. S., Diansky, N. A., Gusev, A. V., Iakovlev, N. G., Shestakova, A. A., and Emelina, S. V.: Simulation of the modern climate using the INM-CM48 climate model, *Russ. J. Numer. Anal. M.*, 33, 367–374, <https://doi.org/10.1515/rnam-2018-0032>, 2018.
- Walker, G. and Bliss, E.: World Weather V, *Mem. R. Metrol. Soc.*, 4, 53–84, 1932.
- Wang, L. and Ting, M.: Stratosphere-Troposphere Coupling Leading to Extended Seasonal Predictability of Summer North Atlantic Oscillation and Boreal Climate, *Geophys. Res. Lett.*, 49, e2021GL096362, <https://doi.org/10.1029/2021GL096362>, 2022.
- Waskom, M. L.: seaborn: statistical data visualization, *Journal of Open Source Software*, 6, 3021, <https://doi.org/10.21105/joss.03021>, 2021.
- Williams, K. D., Copsey, D., Blockley, E. W., Bodas-Salcedo, A., Calvert, D., Comer, R., Davis, P., Graham, T., Hewitt, H. T., Hill, R., Hyder, P., Ineson, S., Johns, T. C., Keen, A. B., Lee, R. W., Megann, A., Milton, S. F., Rae, J. G. L., Roberts, M. J., Scaife, A. A., Schiemann, R., Storkey, D., Thorpe, L., Watterson, I. G., Walters, D. N., West, A., Wood, R. A., Woollings, T., and Xavier, P. K.: The Met Office Global Coupled Model 3.0 and 3.1 (GC3.0

- and GC3.1) Configurations, *J. Adv. Model. Earth Sy.*, 10, 357–380, <https://doi.org/10.1002/2017MS001115>, 2018.
- Woollings, T., Czuchnicki, C., and Franzke, C.: Twentieth century North Atlantic jet variability, *Q. J. Roy. Meteor. Soc.*, 140, 783–791, <https://doi.org/10.1002/qj.2197>, 2014.
- Woollings, T., Franzke, C., Hodson, D. L. R., Dong, B., Barnes, E. A., Raible, C. C., and Pinto, J. G.: Contrasting interannual and multidecadal NAO variability, *Clim. Dynam.*, 45, 539–556, <https://doi.org/10.1007/s00382-014-2237-y>, 2015.
- Xin, X., Wu, T., Li, J., Wang, Z., Li, W., and Wu, F.: How Well does BCC\_CSM1.1 Reproduce the 20th Century Climate Change over China?, *Atmos. Ocean. Sc. Lett.*, 6, 21–26, <https://doi.org/10.1080/16742834.2013.11447053>, 2013.
- Yoshimori, M. and Suzuki, M.: The relevance of mid-Holocene Arctic warming to the future, *Clim. Past*, 15, 1375–1394, <https://doi.org/10.5194/cp-15-1375-2019>, 2019.
- Yukimoto, S., Adachi, Y., Hosaka, M., Sakami, T., Yoshimura, H., Hirabara, M., Tanaka, T. Y., Shindo, E., Tsujino, H., Deushi, M., Mizuta, R., Yabu, S., Obata, A., Nakano, H., Koshiro, T., Ose, T., and Kitoh, A.: A new global climate model of the Meteorological Research Institute: MRI-CGCM3 – model description and basic performance, *J. Meteorol. Soc. Jpn. Ser. II*, 90, 23–64, <https://doi.org/10.2151/jmsj.2012-A02>, 2012.
- Yukimoto, S., Kawai, H., Koshiro, T., Oshima, N., Yoshida, K., Urakawa, S., Tsujino, H., Deushi, M., Tanaka, T., Hosaka, M., Yabu, S., Yoshimura, H., Shindo, E., Mizuta, R., Obata, A., Adachi, Y., and Ishii, M.: The Meteorological Research Institute Earth System Model Version 2.0, MRI-ESM2.0: Description and Basic Evaluation of the Physical Component, *J. Meteorol. Soc. Jpn. Ser. II*, 97, 931–965, <https://doi.org/10.2151/jmsj.2019-051>, 2019.
- Zelinka, M. D., Myers, T. A., McCoy, D. T., Po-Chedley, S., Caldwell, P. M., Ceppi, P., Klein, S. A., and Taylor, K. E.: Causes of Higher Climate Sensitivity in CMIP6 Models, *Geophys. Res. Lett.*, 47, e2019GL085782, <https://doi.org/10.1029/2019GL085782>, 2020.
- Zhang, Q., Liu, B., Li, S., and Zhou, T.: Understanding Models' Global Sea Surface Temperature Bias in Mean State: From CMIP5 to CMIP6, *Geophys. Res. Lett.*, 50, e2022GL100888, <https://doi.org/10.1029/2022GL100888>, 2023.
- Zhang, W., Wang, L., Xiang, B., Qi, L., and He, J.: Impacts of two types of La Niña on the NAO during boreal winter, *Clim. Dynam.*, 44, 1351–1366, <https://doi.org/10.1007/s00382-014-2155-z>, 2015.
- Zhang, W., Wang, Z., Stuecker, M. F., Turner, A. G., Jin, F.-F., and Geng, X.: Impact of ENSO longitudinal position on teleconnections to the NAO, *Clim. Dynam.*, 52, 257–274, <https://doi.org/10.1007/s00382-018-4135-1>, 2019.
- Zhao, A.: `annizhao1994/PMIP_NAO: PMIP_NAO_plottingscripts (v1.1)`, Zenodo [code], <https://doi.org/10.5281/zenodo.15624480>, 2026.
- Zhao, A., Brierley, C. M., Jiang, Z., Eyles, R., Oyarzún, D., and Gomez-Dans, J.: Analysing the PMIP4-CMIP6 collection: a workflow and tool (`pmip_p2fvar_analyzer v1`), *Geosci. Model Dev.*, 15, 2475–2488, <https://doi.org/10.5194/gmd-15-2475-2022>, 2022.
- Zhu, C., Liu, Z., Zhang, S., and Wu, L.: Likely accelerated weakening of Atlantic overturning circulation emerges in optimal salinity fingerprint, *Nat. Commun.*, 14, 1245, <https://doi.org/10.1038/s41467-023-36288-4>, 2023.